Nonlinear Dyn (2014) 76:1611–1632
DOI 10.1007/s11071-013-1233-9

ORIGINAL PAPER

Optimal nonlinear feedback control of spacecraft rendezvous with finite low thrust between libration orbits

Haijun Peng · Xin Jiang · Biaosong Chen

Received: 23 August 2013 / Accepted: 30 December 2013 / Published online: 21 January 2014

Abstract This paper presents the nonlinear closed-loop feedback control strategy for the spacecraft rendezvous problem with finite low thrust between libration orbits in the Sun–Earth system. The model of spacecraft rendezvous takes the perturbations in initial states, the actuator saturation limits, the measurement errors, and the external disturbance forces into consideration from an engineering point of view. The proposed nonlinear closed-loop feedback control strategy is not analytically explicit; rather, it is implemented by a rapid re-computation of the open-loop optimal control at each update instant. To guarantee the computational efficiency, a novel numerical algorithm for solving the open-loop optimal control is given. With the aid of the quasilinearization method, the open-loop optimal control problem is replaced successfully by a series of sparse symmetrical linear equations coupled with linear complementary problem, and the computational efficiency can be significantly increased. The numerical simulations of spacecraft rendezvous problems in the paper well demonstrate the robustness, high precision, and dominant real-time merits of the proposed closed-loop feedback control strategy.

H. Peng (✉) · X. Jiang · B. Chen
Department of Engineering Mechanics, State Key Laboratory of Structural Analysis for Industrial Equipment, Dalian University of Technology, Dalian 116024, China
e-mail: hjpeng@dlut.edu.cn

Keywords Spacecraft rendezvous · Circular restricted three-body problem · Optimal feedback control · Finite low thrust · Libration point orbits

1 Introduction

The exploration of deep space, especially the exploration of libration point space environment, as a hot and important research topic has attracted lots of engineers and researchers in recent years. Because the libration points of the circular restricted three-body problem (CRTBP) represent a series of five points where the gravitational and centrifugal forces are in balance, these space positions are ideal choice for the possibility of settling space stations, a set of interferometer space telescopes, and midway refueling space stations for large missions [1–3]. Therefore, one typical and important problem for space stations or gateway is the autonomous and high accuracy of spacecraft rendezvous on libration point orbits. Successful spacecraft rendezvous is essential for many astronautic missions such as intercepting, repair, rescue, docking, and large-scale structure assembling [4,5].

Although there have been many successful missions and research results for spacecraft rendezvous near the Earth orbits [4–7], the spacecraft rendezvous problem has not been implemented and fully investigated on libration orbits. The spacecraft rendezvous near the Earth orbits, which employs two-body dynamics model is significantly different from that on libra-

tion orbits. Based on the CRTBP model, libration point orbits compared with Kepler orbits have different orbital periods, and the relative velocity of the two spacecraft is also different. The previous works of spacecraft rendezvous on Kepler orbits cannot apply to libration point orbits [8]. In order to fulfill requirement of the autonomous and high accuracy of spacecraft rendezvous on libration point orbits, the control of spacecraft rendezvous should consider the nonlinear character of the CRTBP. Reference [8] employed variable-specific-impulse technology to design optimal rendezvous trajectories between Halo orbits, and discussed influence of the independent parameters and rendezvous time for spacecraft rendezvous. In Ref. [9], the minimum propellant optimal maneuvers of space vehicles equipped with low-thrust propulsion installation for rendezvous in the Earth–moon system are examined. Similarly, the nonlinear problem of the optimal libration points rendezvous in Earth–moon system is examined in Ref. [10]. For rapid computation of optimal trajectory of halo orbit rendezvous in real time, Ref. [11] employed surrogate-based parameter optimization strategy for the optimal trajectory of halo orbit rendezvous in the Sun–Earth system.

However, the above works mainly employ open-loop optimal control for spacecraft rendezvous on libration point orbits. Because the collinear libration point orbits are inherently unstable, a spacecraft with a little deviation from the accurate initial conditions will depart from the desired orbits after a period of time. Furthermore, the gravitational forces from other celestial bodies [12], the navigational error or the measurement error [13], the actuator saturation limits [14], the thrust nonlinearity [15], etc., are inevitably introduced in the real environments of spacecraft rendezvous on libration point orbits. Thus, the objectiveness and performance of autonomous and high accuracy for spacecraft rendezvous are degraded by employing open-loop optimal control in the above situations. On the contrary, the closed-loop feedback controller uses the feedback information to counteract the effects of external disturbances and modeling errors [16–18]. Especially, the method proposed in Ref. [19] which is based on the feedback loop control with a time delay has a potential application of the nonlinear closed-loop feedback control of a periodic orbit. Therefore, the closed-loop feedback control strategy has more advantages than the open-loop control for spacecraft rendezvous in the above situations. However, the closed-loop feedback control problem which considers the finite control input and the nonlinear model of CRTBP have seldom been studied for spacecraft rendezvous between libration orbits till now, and this motivates our work in this paper.

In this paper, the optimal feedback control problem of spacecraft rendezvous between libration orbits is considered that the rendezvous of two spacecrafts starting on Halo orbits of different z amplitudes in the Sun–Earth system around L_2 libration point by using continuous finite low thrust. The pursuit spacecraft leaves a Halo orbit to capture an objective spacecraft on another Halo orbit. Meanwhile, the objective spacecraft is assumed to be nominally coasting along its prescribed Halo orbits. Furthermore, an attempt is made to provide a robust and efficient nonlinear closed-loop feedback control strategy for spacecraft rendezvous with finite time in the presence of external disturbances and control constraints.

The contributions of this paper are several folds: the first of these is the nonlinearities in the dynamical model, and the mission-related control constraints are taken into consideration. The second point is to introduce the initial state errors, the gravitational forces of the moon and the navigational errors in feedback control and to address the difficulties in spacecraft rendezvous between libration orbits. To this end, we circumvent the traditional problems which track a pre-computed spacecraft rendezvous trajectory. The closed-loop feedback control scheme proposed in this paper rapidly resolves the open-loop nonlinear optimal control problem and updates the control command as soon as a new solution is obtained. The last innovation is a new efficient numerical algorithm for solving open-loop nonlinear optimal control problem. The key idea of the proposed algorithm is to employ quasilinearization method and solve a sequence of resulting sparse symmetrical linear equations with linear complementary problem, and thus the online implementation efficiency must be significantly increased.

The paper is organized as follows: First, the nonlinear mathematical model and control problem statements for spacecraft rendezvous between libration orbits are introduced in Sect. 2. Subsequently, a numerical algorithm for solving nonlinear optimal control with finite control input is proposed in Sect. 3. Then, a closed-loop feedback control strategy based on the fast computation of the open-loop optimal control is given in Sect. 4. In final, the closed-loop feedback control

strategy for spacecraft rendezvous between libration orbits in complex disturbance environment is evaluated through numerical simulations and the robustness and high accuracy/efficiency of the proposed closed-loop feedback control strategy have been shown in Sect. 5.

2 Problem formulation

2.1 Mathematical modeling for spacecraft rendezvous

The problem of spacecraft rendezvous between libration orbits in this paper has been modeled by the equations of motion of the CRTBP. The CRTBP models the motion of a spacecraft moving under the influence of two massive bodies, i.e., the Sun and the Earth in this paper. The orbital motion of the Sun and the Earth is not affected by the spacecraft. The Sun and the Earth are assumed to be in circular orbit around the barycenter of the Sun–Earth system. The reference coordinate frame which is centered on the barycenter rotates at the same rate as the orbital motion of the above two massive bodies. The x-axis extends from the barycenter through the Earth, the z-axis extends in the direction of the angular momentum of the system, and the y-axis completes the right-hand coordinate frame. Because this paper mainly discusses the problem of collinear libration orbits around the L_2 point of the Sun–Earth system, it is convenient to transfer the reference frame from the barycenter of the Sun–Earth system to the L_2 point. The equations describing the motion of the controlled spacecraft may be written in the dimensionless form [11]:

$$\ddot{x} - 2\dot{y} - x = -\frac{(1-\mu)(x+1+1/\gamma)}{\gamma^3 d_1^3} - \frac{\mu(x+1)}{\gamma^3 d_2^3} + \frac{1-\mu+\gamma}{\gamma} + u_x, \tag{1}$$

$$\ddot{y} + 2\dot{x} - y = -\frac{(1-\mu)y}{\gamma^3 d_1^3} - \frac{\mu y}{\gamma^3 d_2^3} + u_y, \tag{2}$$

$$\ddot{z} = -\frac{(1-\mu)z}{\gamma^3 d_1^3} - \frac{\mu z}{\gamma^3 d_2^3} + u_z, \tag{3}$$

where $d_1 = \sqrt{(x+1+1/\gamma)^2 + y^2 + z^2}$ and $d_2 = \sqrt{(x+1)^2 + y^2 + z^2}$. The dot represents time derivative in the rotating frame, μ is the ratio of the Earth mass to the sum of the masses of both the Earth and the Sun, the distance between the Earth and the L_2 point is denoted by γ. Symbols u_x, u_y, and u_z are the control inputs of the controlled spacecraft in x, y, and z directions.

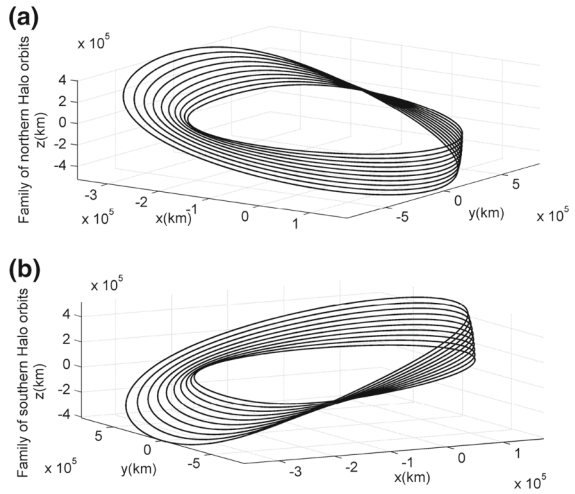

Fig. 1 Families of Halo orbits around the L_2 point in the Sun–Earth system: **a** Northern Halo orbits and **b** Southern Halo orbits

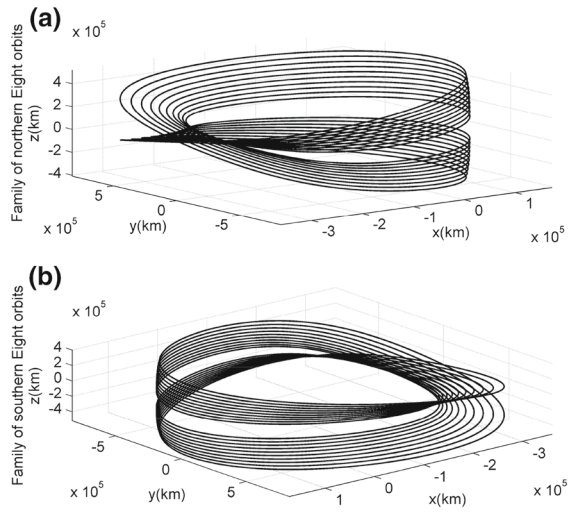

Fig. 2 Families of figure-eight orbits around the L_2 point in the Sun–Earth system: **a** Northern figure-eight orbits and **b** Southern figure-eight orbits.

It is well known that the collinear libration points have families of periodic and quasiperiodic unstable orbits. Halo orbits and figure-eight orbits are special periodic orbits around the collinear libration points, as shown in Figs. 1 and 2. The problem of spacecraft rendezvous is considered in the same and different families of Halo orbits by using continuous finite low thrust in this study.

2.2 Control problem statements

This paper is devoted to find an optimal trajectory and control that guides the pursuit spacecraft from a given Halo orbit to capture the objective spacecraft on another Halo orbit. Therefore, the spacecraft rendezvous problem in terms of optimal control can be stated as: the pursuit spacecraft with the controlled nonlinear differential equation in the form of state space Eq. (4) is derived by continuous finite low thrust $\mathbf{u}$ from the initial state $\mathbf{x}_0$ to the final state $\mathbf{x}_f$

$$\dot{\mathbf{x}}(\tau) = f(\mathbf{x}(\tau), \mathbf{u}(\tau)), \quad \mathbf{x}(\tau = t) = \mathbf{x}_0, \\ \mathbf{x}(\tau = t_f) = \mathbf{x}_f, \tag{4}$$

where $\mathbf{x} = \left[x\ y\ z\ \dot{x}\ \dot{y}\ \dot{z}\right]^T$ is the state variable, $\mathbf{u} = \left[u_x\ u_y\ u_z\right]^T$ is the control variable.

The continuous finite low-thrust control $\mathbf{u}$ can be expressed by the following inequality

$$\underline{\mathbf{u}} \le \mathbf{C}\mathbf{u} \le \bar{\mathbf{u}}, \tag{5}$$

where $\mathbf{C}$ is a constant weighted matrix, and $\bar{\mathbf{u}}$ and $\underline{\mathbf{u}}$ are the upper and lower limits of the control variable $\mathbf{u}$, respectively.

Meanwhile, the following performance index J under the constraints of nonlinear differential Eq. (4) and control inequality Eq. (5) should be minimized

$$J = \frac{1}{2}\int_0^{t_f} \Big[(\mathbf{x} - \mathbf{x}_d)^T \mathbf{Q} (\mathbf{x} - \mathbf{x}_d) \\ + (\mathbf{u} - \mathbf{u}_d)^T \mathbf{R} (\mathbf{u} - \mathbf{u}_d)\Big] d\tau, \tag{6}$$

where $\mathbf{x}_d = \mathbf{x}_f$ and $\mathbf{u}_d$ are the desired states and control inputs during the process of spacecraft rendezvous, respectively. $\mathbf{Q}$ is a positive semidefinite matrix and $\mathbf{R}$ is a positive definite matrix.

The open-loop optimal solution for spacecraft rendezvous can be obtained by solving the above nonlinear optimal control problem Eqs. (4)–(6). In the next section, a numerical algorithm for solving nonlinear optimal control with finite control input will be developed. Furthermore, the closed-loop feedback control strategy will be established based on the open-loop optimal control and various kinds of disturbances will be considered in the spacecraft rendezvous.

3 Numerical algorithm for solving nonlinear optimal control with finite control input

Many numerical methods [20,21] can be used to solve the established nonlinear optimal control problem in the previous section. These numerical methods are divided into two major classes [20,21]: indirect methods and direct methods. The indirect methods transform an optimal control problem into a Hamiltonian boundary-value problem (HBVP) by calculus of variations or the maximum (minimum) principle. In the direct methods, an optimal control problem is discretized and converted into a large-scale parameter optimization problem that can be solved using nonlinear programming methods. However, the open-loop optimal results from these numerical methods cannot fulfill the requirement of spacecraft rendezvous with various kinds of disturbances. Because the indirect methods can conveniently supply the costate information and can be employed to construct closed-loop feedback control, the need for high-performance numerical method for solving HBVP is very urgent and important for the closed-loop feedback control.

One popular method for solving linear HBVP and constructing closed-loop feedback control is the indirect pseudospectral method [17,18,22,23]. The indirect pseudospectral methods expanded the state and costate variables into polynomials with the values of the states and costates at the different discretization points as the expansion coefficients, and then the HBVP are reduced into a system of algebraic equations. For problems where the solutions are infinitely smooth and well behaved, a pseudospectral method has a simple structure and converges at an exponential rate. However, the convergence rate of a pseudospectral method on a problem for which the formulation or solution is nonsmooth may be extremely slow. For example, the inequality constraint of the control input would result in a poor approximation even when a high-degree polynomial is used. In this case, pseudospectral methods exhibit the well-known Gibbs phenomenon resulting from the approximation of a nonsmooth function by a finite number of smooth functions [24]. Also, Ref. [25] has shown that a trigonometric series appear to be "bad working" around the discontinuities due to the Gibbs phenomenon.

To circumvent this issue, the research method appearing in this paper is inspired by an efficient sparse numerical method [26] for solving the linear

receding-horizon control problem. In this way, the linear equation obtained from the above mentioned methods is mostly a large and sparse linear equation with a symmetrical coefficient matrix, and thus the computer memory storage and online implementation efficiency must be significantly optimized. In this paper, this idea is expanded to nonlinear optimal control problem with finite control input. With the aid of the quasilinearization method, the original problem is replaced successfully by a series of linear HBVP coupled with linear complementary problem.

3.1 Problem transcription

To solve the above nonlinear optimal control problem, the quasilinearization method [22] is first applied to expand the controlled nonlinear differential equation and performance index, i.e., unfolding the performance index in the $(k+1)$th iteration, we obtain

$$J^{(k+1)} = \frac{1}{2}\int_0^{t_\mathrm{f}} \left[\left(\mathbf{x}^{(k+1)} - \mathbf{x}_\mathrm{d}\right)^\mathrm{T} \mathbf{Q} \left(\mathbf{x}^{(k+1)} - \mathbf{x}_\mathrm{d}\right) + \left(\mathbf{u}^{(k+1)} - \mathbf{u}_\mathrm{d}\right)^\mathrm{T} \mathbf{R} \left(\mathbf{u}^{(k+1)} - \mathbf{u}_\mathrm{d}\right) \right] \mathrm{d}\tau, \tag{7}$$

subject to

$$\begin{aligned} \dot{\mathbf{x}}^{(k+1)}(\tau) = {} & \mathbf{A}^{(k)}(\tau)\,\mathbf{x}^{(k+1)}(\tau) + \mathbf{B}^{(k)}(\tau)\,\mathbf{u}^{(k+1)}(\tau) \\ & + \mathbf{w}^{(k)}(\tau), \mathbf{x}^{(k+1)}(\tau = t) = \mathbf{x}(t), \\ & \mathbf{x}^{(k+1)}(\tau = t_\mathrm{f}) = \mathbf{x}_\mathrm{f}, \end{aligned} \tag{8}$$

where

$$\begin{cases} \mathbf{A}^{(k)}(\tau) = \left.\frac{\partial f(\mathbf{x}(\tau),\mathbf{u}(\tau))}{\partial \mathbf{x}}\right|_{\mathbf{x}^{(k)}(\tau),\mathbf{u}^{(k)}(\tau)} \\ \mathbf{B}^{(k)}(\tau) = \left.\frac{\partial f(\mathbf{x}(\tau),\mathbf{u}(\tau))}{\partial \mathbf{u}}\right|_{\mathbf{x}^{(k)}(\tau),\mathbf{u}^{(k)}(\tau)} \\ \mathbf{w}^{(k)}(\tau) = f\left(\mathbf{x}^{(k)}(\tau), \mathbf{u}^{(k)}(\tau)\right) - \mathbf{A}^{(k)}(\tau)\,\mathbf{x}^{(k)}(\tau) \\ \qquad -\mathbf{B}^{(k)}(\tau)\,\mathbf{u}^{(k)}(\tau). \end{cases} \tag{9}$$

Symbols $\mathbf{x}^{(k+1)}$ and $\mathbf{u}^{(k+1)}$ are the state and control vectors for the current $(k+1)$th iteration, respectively, and symbols $\mathbf{x}^{(k)}$ and $\mathbf{u}^{(k)}$ are state and control vectors from the previous kth iteration and are taken as the references for the current computation.

By introducing the parameter variables $\bar{\boldsymbol{\alpha}}^{(k+1)}$ and $\underline{\boldsymbol{\alpha}}^{(k+1)}$ in the current $(k+1)$th iteration, Eq. (5) can be transformed into the following constraints

$$\begin{cases} \mathbf{C}\mathbf{u}^{(k+1)} - \bar{\mathbf{u}} + \bar{\boldsymbol{\alpha}}^{(k+1)} = \mathbf{0}; & \bar{\boldsymbol{\alpha}}^{(k+1)} \geq \mathbf{0} \\ \underline{\mathbf{u}} - \mathbf{C}\mathbf{u}^{(k+1)} + \underline{\boldsymbol{\alpha}}^{(k+1)} = \mathbf{0}; & \underline{\boldsymbol{\alpha}}^{(k+1)} \geq \mathbf{0}. \end{cases} \tag{10}$$

Because the inequality constraint Eq. (5) has been transformed into the equality constraint Eq. (10) in the current $(k+1)$th iteration, the Hamiltonian function $\bar{H}^{(k+1)}$ in the $(k+1)$th iteration can be obtained by introducing the Lagrange and parameter multipliers as following

$$\begin{aligned} \bar{H}^{(k+1)} = {} & \frac{1}{2}\left[\left(\mathbf{x}^{(k+1)} - \mathbf{x}_\mathrm{d}\right)^\mathrm{T} \mathbf{Q} \left(\mathbf{x}^{(k+1)} - \mathbf{x}_\mathrm{d}\right) \right. \\ & \left. + \left(\mathbf{u}^{(k+1)} - \mathbf{u}_\mathrm{d}\right)^\mathrm{T} \mathbf{R} \left(\mathbf{u}^{(k+1)} - \mathbf{u}_\mathrm{d}\right) \right] \\ & + \left(\boldsymbol{\lambda}^{(k+1)}\right)^\mathrm{T} \left(\mathbf{A}^{(k)}(\tau)\,\mathbf{x}^{(k+1)} \right. \\ & \left. + \mathbf{B}^{(k)}(\tau)\,\mathbf{u}^{(k+1)} + \mathbf{w}^{(k)}(\tau)\right) \\ & + \left(\bar{\boldsymbol{\beta}}^{(k+1)}\right)^\mathrm{T} \left(\mathbf{C}\mathbf{u}^{(k+1)} - \bar{\mathbf{u}} + \bar{\boldsymbol{\alpha}}^{(k+1)}\right) \\ & + \left(\underline{\boldsymbol{\beta}}^{(k+1)}\right)^\mathrm{T} \left(\underline{\mathbf{u}} - \mathbf{C}\mathbf{u}^{(\mathbf{k+1})} + \underline{\boldsymbol{\alpha}}^{(\mathbf{k+1})}\right), \end{aligned} \tag{11}$$

where $\boldsymbol{\lambda}^{(k+1)}$ are the Lagrange multipliers, and $\bar{\boldsymbol{\beta}}^{(k+1)}$ and $\underline{\boldsymbol{\beta}}^{(k+1)}$ are parameter multipliers in the $(k+1)$th iteration.

According to the principle of optimality, i.e., the Hamiltonian function $\bar{H}^{(k+1)}$ with respect to the control variable $\mathbf{u}^{(k+1)}$, it gives

$$\frac{\partial \bar{H}^{(k+1)}}{\partial \mathbf{u}^{(k+1)}} = \mathbf{0}. \tag{12}$$

Equation (12) gives the following explicit expression of the control variable $\mathbf{u}^{(k+1)}$

$$\begin{aligned} \mathbf{u}^{(k+1)} = {} & \mathbf{u}_\mathrm{d} - \mathbf{R}^{-1}\left[\left(\mathbf{B}^{(k)}(\tau)\right)^\mathrm{T} \boldsymbol{\lambda}^{(k+1)} + \mathbf{C}^\mathrm{T} \bar{\boldsymbol{\beta}}^{(k+1)} \right. \\ & \left. - \mathbf{C}^\mathrm{T} \underline{\boldsymbol{\beta}}^{(k+1)} \right]. \end{aligned} \tag{13}$$

Substituting Eq. (13) into the Hamiltonian function $H^{(k+1)}$ Eq. (11), we obtain a new Hamiltonian function that is only dependent on the state variable, the costate variable, and the parametric variable multipliers. Because the parametric variables $\bar{\boldsymbol{\beta}}^{(k+1)}$ and $\underline{\boldsymbol{\beta}}^{(k+1)}$ are not involved in the variations, some terms in the Hamiltonian function, which are not related to the state and costate variables can be neglected, then a new Hamiltonian function is given by

$$H^{(k+1)} = \frac{1}{2}\left(\mathbf{x}^{(k+1)} - \mathbf{x}_{\mathrm{d}}\right)^{\mathrm{T}} \mathbf{Q}\left(\mathbf{x}^{(k+1)} - \mathbf{x}_{\mathrm{d}}\right) - \frac{1}{2}\left(\boldsymbol{\lambda}^{(k+1)}\right)^{\mathrm{T}} \mathbf{B}^{(k)}(\tau)\mathbf{R}^{-1}\left(\mathbf{B}^{(k)}(\tau)\right)^{\mathrm{T}} \times \boldsymbol{\lambda}^{(k+1)} + \left(\boldsymbol{\lambda}^{(k+1)}\right)^{\mathrm{T}} \mathbf{A}^{(k)}(\tau)\mathbf{x}^{(k+1)} + \left(\boldsymbol{\lambda}^{(k+1)}\right)^{\mathrm{T}} \mathbf{B}^{(k)}(\tau)\mathbf{u}_{\mathrm{d}} + \left(\boldsymbol{\lambda}^{(k+1)}\right)^{\mathrm{T}} \times \mathbf{w}^{(k)}(\tau) + \left(\boldsymbol{\lambda}^{(k+1)}\right)^{\mathrm{T}} \mathbf{B}^{(k)}(\tau)\mathbf{R}^{-1}\mathbf{C}^{\mathrm{T}} \times \left(\underline{\boldsymbol{\beta}}^{(k+1)} - \bar{\boldsymbol{\beta}}^{(k+1)}\right). \tag{14}$$

Based on the variational principle, the necessary condition for optimal control is

$$\delta_{\mathbf{x},\boldsymbol{\lambda}} \int_0^{t_{\mathrm{f}}} H^{(k+1)} \mathrm{d}\tau = 0, \tag{15}$$

where $\delta_{\mathbf{x},\boldsymbol{\lambda}}$ denotes the calculus of variations with respect to the state variable $\mathbf{x}$ and the costate variable λ. Substituting Eq. (14) into Eq. (15) gives the following Hamiltonian canonical equations

$$\dot{\mathbf{x}}^{(k+1)} = \frac{\partial H^{(k+1)}}{\partial \boldsymbol{\lambda}^{(k+1)}} = \mathbf{A}^{(k)}(\tau)\mathbf{x}^{(k+1)} - \mathbf{B}^{(k)}(\tau)\mathbf{R}^{-1} \times \left(\mathbf{B}^{(k)}(\tau)\right)^{\mathrm{T}} \boldsymbol{\lambda}^{(k+1)} + \mathbf{B}^{(k)}(\tau)\mathbf{u}_{\mathrm{d}} + \mathbf{w}^{(k)}(\tau) + \mathbf{B}^{(k)}(\tau)\mathbf{R}^{-1}\mathbf{C}^{\mathrm{T}} \times \left(\underline{\boldsymbol{\beta}}^{(k+1)} - \bar{\boldsymbol{\beta}}^{(k+1)}\right), \tag{16}$$

$$\dot{\boldsymbol{\lambda}}^{(k+1)} = -\frac{\partial H^{(k+1)}}{\partial \mathbf{x}^{(k+1)}} = -\mathbf{Q}\mathbf{x}^{(k+1)} - \left(\mathbf{A}^{(k)}(\tau)\right)^{\mathrm{T}} \boldsymbol{\lambda}^{(k+1)} + \mathbf{Q}\mathbf{x}_{\mathrm{d}}, \tag{17}$$

with the following boundary condition

$$\mathbf{x}^{(k+1)}(\tau = t) = \mathbf{x}_0, \tag{18}$$

$$\mathbf{x}^{(k+1)}(\tau = t_{\mathrm{f}}) = \mathbf{x}_{\mathrm{f}}. \tag{19}$$

Meanwhile, the nonlinear optimal control problem should satisfy the equality constraint given by Eq. (10). With Eq. (13), the equality constraint in the $(k+1)$th iteration can be rewritten as

$$\bar{\boldsymbol{\alpha}}^{(k+1)} + \mathbf{C}\mathbf{u}_{\mathrm{d}} + \mathbf{C}\mathbf{R}^{-1}\left(-\mathbf{B}(\tau)\boldsymbol{\lambda}^{(k+1)} - \mathbf{C}^{\mathrm{T}}\bar{\boldsymbol{\beta}}^{(k+1)} + \mathbf{C}^{\mathrm{T}}\underline{\boldsymbol{\beta}}^{(k+1)}\right) - \bar{\mathbf{u}} = \mathbf{0}, \tag{20}$$

$$\underline{\boldsymbol{\alpha}}^{(k+1)} - \mathbf{C}\mathbf{u}_{\mathrm{d}} - \mathbf{C}\mathbf{R}^{-1}\left(-\mathbf{B}(\tau)\boldsymbol{\lambda}^{(k+1)} - \mathbf{C}^{\mathrm{T}}\bar{\boldsymbol{\beta}}^{(k+1)} + \mathbf{C}^{\mathrm{T}}\underline{\boldsymbol{\beta}}^{(k+1)}\right) + \mathbf{u} = \mathbf{0}. \tag{21}$$

Furthermore, the variables $\bar{\boldsymbol{\alpha}}^{(k+1)}$, $\underline{\boldsymbol{\alpha}}^{(k+1)}$, $\bar{\boldsymbol{\beta}}^{(k+1)}$, $\underline{\boldsymbol{\beta}}^{(k+1)}$ should satisfy the linear complementarity conditions as shown

$$\bar{\boldsymbol{\alpha}}^{(k+1)} \geq \mathbf{0},\ \bar{\boldsymbol{\beta}}^{(k+1)} \geq \mathbf{0},\ \left(\bar{\boldsymbol{\alpha}}^{(k+1)}\right)^{\mathrm{T}} \bar{\boldsymbol{\beta}}^{(k+1)} = \mathbf{0}, \tag{22}$$

$$\underline{\boldsymbol{\alpha}}^{(k+1)} \geq \mathbf{0},\ \underline{\boldsymbol{\beta}}^{(k+1)} \geq \mathbf{0},\ \left(\underline{\boldsymbol{\alpha}}^{(k+1)}\right)^{\mathrm{T}} \underline{\boldsymbol{\beta}}^{(k+1)} = \mathbf{0}. \tag{23}$$

Based on the above analysis, the original nonlinear optimal control problem with finite control input has been transformed into the iteration form of Hamiltonian boundary-value problem coupled with linear complementary problem. In each iteration step, the Hamiltonian boundary-value problem can be expressed by Eqs. (16)–(19), while the linear complementary problem can be expressed by Eqs. (20)–(23). In the following section, we are going to develop a discretization scheme to simplify the continuous Hamiltonian boundary-value problem, while in Sect. 3.3 the continuous linear complementary problem will also be added into the discretization scheme and the whole coupled problem can be solved in a uniform discretization format.

3.2 Discretization scheme

In order to formulate discretization scheme conveniently and clearly, all the problems are considered within the $(k+1)$th iteration step in this and the following sections. Meanwhile, the symbol superscript $(k+1)$ has been ignored. So, a discretization scheme will be introduced and the linear HBVP will be transformed into the solution of linear algebraic equations.

Within a continuous time interval (t, t_{f}), the fourth kind of generating function can be defined as [27,28]

$$V = \boldsymbol{\lambda}_t^{\mathrm{T}}\mathbf{x}_t - \boldsymbol{\lambda}_{t_{\mathrm{f}}}^{\mathrm{T}}\mathbf{x}_{t_{\mathrm{f}}} + \bar{S}, \tag{24}$$

where $\mathbf{x}_t$ and $\boldsymbol{\lambda}_t$ are the state and costate variables at the initial time, respectively. $\mathbf{x}_{t_{\mathrm{f}}}$ and $\boldsymbol{\lambda}_{t_{\mathrm{f}}}$ are the

state and costate variables at the terminal time t_{f}, respectively. Moreover, the fourth kind of generating function V is only the function of costates λ_t and $\boldsymbol{\lambda}_{t_{\mathrm{f}}}$, and the action $\bar{S}$ is defined by

$$\bar{S} = \int_{t}^{t_{\mathrm{f}}} \left(\boldsymbol{\lambda}^{\mathrm{T}}\dot{\mathbf{x}} - H\right)\mathrm{d}\tau, \tag{25}$$

where H is a Hamiltonian function expressed as Eq. (14).

Because the calculus of variations for the action $\bar{S}$ can give the Hamiltonian canonical Eq. [26] and if the Hamiltonian canonical equation is satisfied in the time interval (t, t_{f}), the differential quotient for generating function can be derived based on Eq. (24) as

$$\mathrm{d}V = \mathbf{x}_t^{\mathrm{T}}\mathrm{d}\boldsymbol{\lambda}_t - \mathbf{x}_{t_{\mathrm{f}}}^{\mathrm{T}}\mathrm{d}\boldsymbol{\lambda}_{t_{\mathrm{f}}}. \tag{26}$$

Equation (26) implies that if the Hamiltonian canonical equations are satisfied within the time interval (t, t_{f}) and the costate variable $\boldsymbol{\lambda}_t$ and $\boldsymbol{\lambda}_{t_{\mathrm{f}}}$ at two ends of the time interval are taken as the independent variables, the generating function V must be a function of only $\boldsymbol{\lambda}_t$ and $\boldsymbol{\lambda}_{t_{\mathrm{f}}}$. Therefore, in the following analysis, based on Eq. (26) and taking costate variables at two ends as the independent variables, a numerical approach for solving the HBVP is proposed.

For a numerical approach, the continuous time domain $\tau \in (t, t_{\mathrm{f}})$ is divided into N time intervals with equal time step $\eta = (t_{\mathrm{f}} - t)/N$, i.e.,

$$t_0 = t,\ t_1 = t + \eta,\ \ldots,\ t_j = t + j\eta,\ \ldots,\ t_N = t_{\mathrm{f}}. \tag{27}$$

The numerical approach can be constructed to be compatible with Eq. (26) as follows: assuming that within the j th sub-interval $\left(t_{j-1},\ t_j\right)$, the state variable $\mathbf{x}(\tau)$ is approximated by Lagrange polynomials of degree $r-1$ that interpolate r equidistant points, and the costate variable $\boldsymbol{\lambda}(\tau)$ is approximated by Lagrange polynomials of degree $s-1$ that interpolate s equidistant points, i.e.,

$$\mathbf{x}(\tau) = (\mathbf{M} \otimes \mathbf{I})\,\bar{\boldsymbol{x}}_j, \tag{28}$$

$$\boldsymbol{\lambda}(\tau) = N_1\boldsymbol{\lambda}_{j-1} + \left(\underline{\mathbf{N}} \otimes \mathbf{I}\right)\bar{\boldsymbol{\lambda}}_j + N_n\boldsymbol{\lambda}_j, \tag{29}$$

where $\mathbf{I}$ denotes a $d \times d$ identity matrix, vectors λ_{j-1} and $\boldsymbol{\lambda}_j$ denote the costate variables at the left end and the right end of the j th sub-interval, respectively, vector $\bar{\mathbf{x}}_j$ is defined by $\bar{\mathbf{x}}_j = \left\{\left(\bar{\mathbf{x}}_j^1\right)^{\mathrm{T}}, \left(\bar{\mathbf{x}}_j^2\right)^{\mathrm{T}}, \cdots, \left(\bar{\mathbf{x}}_j^m\right)^{\mathrm{T}}\right\}^{\mathrm{T}}$, and $\bar{\boldsymbol{\lambda}}_j$ is defined by $\bar{\boldsymbol{\lambda}}_j = \left\{\left(\bar{\boldsymbol{\lambda}}_j^2\right)^{\mathrm{T}}, \left(\bar{\boldsymbol{\lambda}}_j^3\right)^{\mathrm{T}}, \ldots, \left(\bar{\boldsymbol{\lambda}}_j^{n-1}\right)^{\mathrm{T}}\right\}^{\mathrm{T}}$. Other symbols in Eqs. (28) and (29) are defined as

$$\mathbf{M} = [M_1, M_2, \ldots, M_r], \tag{30}$$

$$\underline{\mathbf{N}} = \left[N_2, N_3, \ldots, N_{s-1}\right], \tag{31}$$

$$M_i = \prod_{j=1, j\neq i}^{r} \frac{\tau - \tau_j}{\tau_i - \tau_j}, \tag{32}$$

$$N_i = \prod_{j=1, j\neq i}^{s} \frac{\tau - \tau_j}{\tau_i - \tau_j}. \tag{33}$$

The symbol $\otimes$ in Eqs. (28) and (29) denotes the Kronecker product of two matrices. Substituting the approximate state and costate variables, i.e., Eqs. (28) and (29), into Eq. (24) yields

$$\begin{aligned} &V_j\left(\boldsymbol{\lambda}_{j-1}, \boldsymbol{\lambda}_j, \bar{\mathbf{x}}_j, \bar{\boldsymbol{\lambda}}_j\right) \\ &= \boldsymbol{\lambda}_{j-1}^{\mathrm{T}}\bar{\mathbf{x}}_j^1 - \boldsymbol{\lambda}_j^{\mathrm{T}}\bar{\mathbf{x}}_j^m + \int_{t_{j-1}}^{t_j} \left(\boldsymbol{\lambda}^{\mathrm{T}}\dot{\mathbf{x}} - H(\mathbf{x}, \boldsymbol{\lambda})\right)\mathrm{d}\tau. \end{aligned} \tag{34}$$

For the brevity of expression, the following formulae are defined:

$$\begin{aligned} \mathbf{F}_1^j = \frac{\partial V_j}{\partial \boldsymbol{\lambda}_{j-1}} &= \mathbf{K}_{11}^j\boldsymbol{\lambda}_{j-1} + \left(\mathbf{E}_u^{\mathrm{T}} + \mathbf{K}_{12}^j\right)\bar{\mathbf{x}}_j \\ &+ \mathbf{K}_{13}^j\bar{\boldsymbol{\lambda}}_j + \mathbf{K}_{14}^j\boldsymbol{\lambda}_j + \mathbf{f}_{\mathbf{1}}^{\mathbf{j}}, \end{aligned} \tag{35}$$

$$\begin{aligned} \mathbf{F}_2^j = \frac{\partial V_j}{\partial \bar{\mathbf{x}}_j} &= \left(\mathbf{K}_{21}^j + \mathbf{E}_u\right)\boldsymbol{\lambda}_{j-1} - \mathbf{K}_{22}^j\bar{\mathbf{x}}_j + \mathbf{K}_{23}^j\bar{\boldsymbol{\lambda}}_j \\ &+ \left(\mathbf{K}_{24}^j - \mathbf{E}_{\mathrm{d}}\right)\boldsymbol{\lambda}_j + \mathbf{f}_{\mathbf{2}}^{\mathbf{j}}, \end{aligned} \tag{36}$$

$$\begin{aligned} \mathbf{F}_3^j = \frac{\partial V_j}{\partial \bar{\boldsymbol{\lambda}}_j} &= \mathbf{K}_{31}^j\lambda_{j-1} + \mathbf{K}_{32}^j\bar{\mathbf{x}}_j + \mathbf{K}_{33}^j\bar{\boldsymbol{\lambda}}_j \\ &+ \mathbf{K}_{34}^j\boldsymbol{\lambda}_j + \mathbf{f}_{\mathbf{3}}^{\mathbf{j}}, \end{aligned} \tag{37}$$

$$\begin{aligned} \mathbf{F}_4^j = \frac{\partial V_j}{\partial \boldsymbol{\lambda}_j} &= \mathbf{K}_{41}^j\boldsymbol{\lambda}_{j-1} + \left(\mathbf{K}_{42}^j - \mathbf{E}_{\mathrm{d}}^{\mathrm{T}}\right)\bar{\mathbf{x}}_j \\ &+ \mathbf{K}_{43}^j\bar{\boldsymbol{\lambda}}_j + \mathbf{K}_{44}^j\boldsymbol{\lambda}_j + \mathbf{f}_{\mathbf{4}}^{\mathbf{j}}, \end{aligned} \tag{38}$$

$$\mathbf{E}_u = \left[\mathbf{I}\ \mathbf{0}\ \cdots\ \mathbf{0}\right]^{\mathrm{T}}, \tag{39}$$

$$\mathbf{E}_{\mathrm{d}} = \left[\mathbf{0}\ \cdots\ \mathbf{0}\ \mathbf{I}\right]^{\mathrm{T}}. \tag{40}$$

The detailed expressions for $\mathbf{K}_{u,v}^{j}$ $(u, v = 1, 2, 3, 4)$ and $\mathbf{f}_{i}^{j}$ $(i = 1, 2, 3, 4)$ in Eqs. (35)–(38) can be found in the Appendix.

According to Eq. (26), if the costate variables $\boldsymbol{\lambda}_{j-1}$ and $\boldsymbol{\lambda}_{j}$ at the two ends of the jth sub-interval are taken as the independent variables and the Hamiltonian canonical equation is satisfied within the j th sub-interval, $V_j(\boldsymbol{\lambda}_{j-1}, \boldsymbol{\lambda}_j, \bar{\mathbf{x}}_j, \bar{\boldsymbol{\lambda}}_j)$ must be a function of only the costate variables at the two ends of the j th sub-interval. Therefore, the following equations must be satisfied

$$\mathbf{F}_2^j = \frac{\partial V_j(\boldsymbol{\lambda}_{j-1}, \boldsymbol{\lambda}_j, \bar{\mathbf{x}}_j, \bar{\boldsymbol{\lambda}}_j)}{\partial \bar{\mathbf{x}}_j} = \mathbf{0}, \tag{41}$$

$$\mathbf{F}_3^j = \frac{\partial V_j(\boldsymbol{\lambda}_{j-1}, \boldsymbol{\lambda}_j, \bar{\mathbf{x}}_j, \bar{\boldsymbol{\lambda}}_j)}{\partial \bar{\boldsymbol{\lambda}}_j} = \mathbf{0}. \tag{42}$$

By solving Eqs. (41) and (42), the dependent variables $\bar{\mathbf{x}}_j$ and $\bar{\boldsymbol{\lambda}}_j$ can be expressed by the independent variables $\boldsymbol{\lambda}_{j-1}$ and $\boldsymbol{\lambda}_j$ as

$$\begin{aligned}\bar{\mathbf{x}}_j = {} & \left(\mathbf{K}_{22}^j\right)^{-1}\left[\left(\mathbf{K}_{24}^j - \mathbf{E}_{\mathrm{d}}\right) - \mathbf{K}_{23}^j\left(\mathbf{K}_{aa}^j\right)^{-1}\left(\mathbf{K}_{bb}^j + \mathbf{K}_{34}^j\right)\right]\boldsymbol{\lambda}_j \\ & + \left(\mathbf{K}_{22}^j\right)^{-1}\left[\left(\mathbf{K}_{21}^j + \mathbf{E}_u\right) - \mathbf{K}_{23}^j\left(\mathbf{K}_{aa}^j\right)^{-1}\left(\mathbf{K}_{cc}^j + \mathbf{K}_{31}^j\right)\right]\boldsymbol{\lambda}_{j-1} \\ & - \left(\mathbf{K}_{22}^j\right)^{-1}\mathbf{K}_{23}^j\left(\mathbf{K}_{aa}^j\right)^{-1}\mathbf{K}_{32}^j\left(\mathbf{K}_{22}^j\right)^{-1}\mathbf{f}_2^j - \left(\mathbf{K}_{22}^j\right)^{-1}\mathbf{K}_{23}^j\left(\mathbf{K}_{aa}^j\right)^{-1}\mathbf{f}_3^j + \left(\mathbf{K}_{22}^j\right)^{-1}\mathbf{f}_2^j, \end{aligned} \tag{43}$$

$$\bar{\boldsymbol{\lambda}}_j = -\left(\mathbf{K}_{aa}^j\right)^{-1}\left(\mathbf{K}_{bb}^j + \mathbf{K}_{34}^j\right)\boldsymbol{\lambda}_j - \left(\mathbf{K}_{aa}^j\right)^{-1}\left(\mathbf{K}_{cc}^j + \mathbf{K}_{31}^j\right)\boldsymbol{\lambda}_{j-1} - \left(\mathbf{K}_{aa}^j\right)^{-1}\mathbf{K}_{32}^j\left(\mathbf{K}_{22}^j\right)^{-1}\mathbf{f}_2^j - \left(\mathbf{K}_{aa}^j\right)^{-1}\mathbf{f}_3^j, \tag{44}$$

where

$$\mathbf{K}_{aa}^j = \mathbf{K}_{33}^j + \mathbf{K}_{32}^j\left(\mathbf{K}_{22}^j\right)^{-1}\mathbf{K}_{23}^j, \tag{45}$$

$$\mathbf{K}_{bb}^j = \mathbf{K}_{32}^j\left(\mathbf{K}_{22}^j\right)^{-1}\left(\mathbf{K}_{24}^j - \mathbf{E}_{\mathrm{d}}\right), \tag{46}$$

$$\mathbf{K}_{cc}^j = \mathbf{K}_{32}^j\left(\mathbf{K}_{22}^j\right)^{-1}\left(\mathbf{K}_{21}^j + \mathbf{E}_u\right). \tag{47}$$

Accordingly, substituting the dependent variables $\bar{\mathbf{x}}_j$ and $\bar{\boldsymbol{\lambda}}_j$, i.e., Eqs. (43) and (44), into Eqs. (35) and (38) produces

$$\mathbf{F}_1^j = \mathbf{S}_{11}^j\boldsymbol{\lambda}_{j-1} + \mathbf{S}_{12}^j\boldsymbol{\lambda}_j + \boldsymbol{\zeta}_1^j, \tag{48}$$

$$\mathbf{F}_4^j = \mathbf{S}_{21}^j\boldsymbol{\lambda}_{j-1} + \mathbf{S}_{22}^j\boldsymbol{\lambda}_j + \boldsymbol{\zeta}_2^j, \tag{49}$$

where

$$\begin{aligned}\mathbf{S}_{11}^j = {} & \mathbf{K}_{11}^j + \left(\mathbf{E}_u^{\mathrm{T}} + \mathbf{K}_{12}^j\right)\left(\mathbf{K}_{22}^j\right)^{-1}\left(\mathbf{K}_{21}^j + \mathbf{E}_u\right) \\ & - \left(\mathbf{K}_{13}^j + \left(\mathbf{K}_{cc}^j\right)^{\mathrm{T}}\right)\left(\mathbf{K}_{aa}^j\right)^{-1}\left(\mathbf{K}_{31}^j + \mathbf{K}_{cc}^j\right), \end{aligned} \tag{50}$$

$$\begin{aligned}\mathbf{S}_{12}^j = {} & \mathbf{K}_{14}^j + \left(\mathbf{E}_u^{\mathrm{T}} + \mathbf{K}_{12}^j\right)\left(\mathbf{K}_{22}^j\right)^{-1}\left(\mathbf{K}_{24}^j - \mathbf{E}_{\mathrm{d}}\right) \\ & - \left(\mathbf{K}_{13}^j + \left(\mathbf{K}_{cc}^j\right)^{\mathrm{T}}\right)\left(\mathbf{K}_{aa}^j\right)^{-1}\left(\mathbf{K}_{34}^j + \mathbf{K}_{bb}^j\right), \end{aligned} \tag{51}$$

$$\begin{aligned}\mathbf{S}_{21}^j = {} & \mathbf{K}_{41}^j + \left(\mathbf{K}_{42}^j - \mathbf{E}_{\mathrm{d}}^{\mathrm{T}}\right)\left(\mathbf{K}_{22}^j\right)^{-1}\left(\mathbf{K}_{21}^j + \mathbf{E}_u\right) \\ & - \left(\mathbf{K}_{43}^j + \left(\mathbf{K}_{bb}^j\right)^{\mathrm{T}}\right)\left(\mathbf{K}_{aa}^j\right)^{-1}\left(\mathbf{K}_{31}^j + \mathbf{K}_{cc}^j\right), \end{aligned} \tag{52}$$

$$\begin{aligned}\mathbf{S}_{22}^j = {} & \mathbf{K}_{44}^j + \left(\mathbf{K}_{42}^j - \mathbf{E}_{\mathrm{d}}^{\mathrm{T}}\right)\left(\mathbf{K}_{22}^j\right)^{-1}\left(\mathbf{K}_{24}^j - \mathbf{E}_{\mathrm{d}}\right) \\ & - \left(\mathbf{K}_{43}^j + \left(\mathbf{K}_{bb}^j\right)^{\mathrm{T}}\right)\left(\mathbf{K}_{aa}^j\right)^{-1}\left(\mathbf{K}_{34}^j + \mathbf{K}_{bb}^j\right), \end{aligned} \tag{53}$$

$$\begin{aligned}\boldsymbol{\zeta}_1^j = {} & -\left(\mathbf{E}_u^{\mathrm{T}} + \mathbf{K}_{12}^j\right)\left(\mathbf{K}_{22}^j\right)^{-1}\mathbf{K}_{dd}^j \\ & -\mathbf{K}_{13}^j\left(\mathbf{K}_{aa}^j\right)^{-1}\mathbf{K}_{ee}^j + \mathbf{f}_1^j, \end{aligned} \tag{54}$$

$$\begin{aligned}\boldsymbol{\zeta}_2^j = {} & -\left(\mathbf{K}_{42}^j - \mathbf{E}_{\mathrm{d}}^{\mathrm{T}}\right)\left(\mathbf{K}_{22}^j\right)^{-1}\mathbf{K}_{dd}^j \\ & -\mathbf{K}_{43}^j\left(\mathbf{K}_{aa}^j\right)^{-1}\mathbf{K}_{ee}^j + \mathbf{f}_4^j, \end{aligned} \tag{55}$$

$$\begin{aligned}\mathbf{K}_{dd}^j = {} & \mathbf{K}_{23}^j\left(\mathbf{K}_{aa}^j\right)^{-1}\mathbf{K}_{32}^j\left(\mathbf{K}_{22}^j\right)^{-1}\mathbf{f}_2^j \\ & +\mathbf{K}_{23}^j\left(\mathbf{K}_{aa}^j\right)^{-1}\mathbf{f}_3^j - \mathbf{f}_2^j, \end{aligned} \tag{56}$$

$$\mathbf{K}_{ee}^j = \mathbf{K}_{32}^j\left(\mathbf{K}_{22}^j\right)^{-1}\mathbf{f}_2^j + \mathbf{f}_3^j. \tag{57}$$

Rewriting Eqs. (54) and (55) as the following form

$$\boldsymbol{\zeta}_1^j = \boldsymbol{\zeta}_{11}^j - \boldsymbol{\zeta}_{12}^j \left(\underline{\boldsymbol{\beta}}^j - \bar{\boldsymbol{\beta}}^j\right), \tag{58}$$

$$\boldsymbol{\zeta}_2^j = \boldsymbol{\zeta}_{21}^j - \boldsymbol{\zeta}_{22}^j \left(\underline{\boldsymbol{\beta}}^j - \bar{\boldsymbol{\beta}}^j\right). \tag{59}$$

The detailed expressions for $\boldsymbol{\zeta}_{pq}^j$ $(p, q = 1, 2)$ in Eqs. (58) and (59) can be found in the Appendix.

From Eqs. (51) and (52), it can be observed that $\mathbf{S}_{21}^j = \left(\mathbf{S}_{12}^j\right)^{\mathrm{T}}$. In addition, Eq. (26) gives the relationship between the generating function and the costate variables at two ends of time interval (t, t_{f}). If the jth sub-interval $\left(t_{j-1},\ t_j\right)$ is considered, the similar relationship can be rewritten as

$$\mathrm{d}V_j = \mathbf{x}_{j-1}^{\mathrm{T}} \mathrm{d}\boldsymbol{\lambda}_{j-1} - \mathbf{x}_j^{\mathrm{T}} \mathrm{d}\boldsymbol{\lambda}_j. \tag{60}$$

According to Eq. (60), we have the following equations:

$$\frac{\partial V_j}{\partial \boldsymbol{\lambda}_j} + \mathbf{x}_j = \mathbf{0}, \tag{61}$$

$$\frac{\partial V_j}{\partial \boldsymbol{\lambda}_{j-1}} - \mathbf{x}_{j-1} = \mathbf{0}. \tag{62}$$

Using the continuous conditions of two adjacent time interval and the formulae (35)–(38), the governing equations for the whole time domain (t, t_{f}) can be given as

$$\mathbf{F}_1^1 = \mathbf{x}_0, \tag{63}$$

$$\mathbf{F}_4^j + \mathbf{F}_1^{j+1} = \mathbf{0}. \tag{64}$$

Equation (63) represents the initial boundary condition, which is previously showed by Eq. (18). Based on Eqs. (38), (49), and (62), we can obtain

$$\mathbf{x}_j = -\mathbf{F}_4^j = -\mathbf{S}_{21}^j \boldsymbol{\lambda}_{j-1} - \mathbf{S}_{22}^j \boldsymbol{\lambda}\boldsymbol{\lambda}_j - \boldsymbol{\zeta}_2^j. \tag{65}$$

Substituting Eq. (65) into Eq. (19), we can get the following boundary condition that is equivalent to Eq. (19)

$$\mathbf{S}_{21}^N \boldsymbol{\lambda}_{N-1} + \mathbf{S}_{22}^N \boldsymbol{\lambda}_N = -\mathbf{x}_{\mathrm{f}} - \boldsymbol{\zeta}_2^N. \tag{66}$$

Now, based on the variational principle, the Hamiltonian canonical Eqs. (16) and (17) are transformed into a set of linear Eqs. (63), (64), and (66). It is easy to rewrite Eqs. (63), (64), and (66) as the following standard linear equation

$$\mathcal{A}\boldsymbol{\lambda} = \mathcal{B}, \tag{67}$$

where

$$\boldsymbol{\lambda} = \left\{\boldsymbol{\lambda}\left(t_0\right)^{\mathrm{T}}, \boldsymbol{\lambda}\left(t_1\right)^{\mathrm{T}}, \cdots, \boldsymbol{\lambda}\left(t_j\right)^{\mathrm{T}}, \cdots, \boldsymbol{\lambda}\left(t_N\right)^{\mathrm{T}}\right\}^{\mathrm{T}}, \tag{68}$$

$$\mathcal{B} = \left\{(\mathbf{x}_0 - \zeta_1^1)^{\mathrm{T}}, -(\zeta_2^1 + \zeta_1^2)^{\mathrm{T}}, \cdots, -(\zeta_2^j + \zeta_1^{j+1})^{\mathrm{T}}, \right.$$
$$\left. \cdots, -(\zeta_2^{N-1} + \zeta_1^N)^{\mathrm{T}}, -(\zeta_2^N + \mathbf{x}_{\mathrm{f}})^{\mathrm{T}}\right\}^{\mathrm{T}}, \tag{69}$$

$$\mathcal{A} = \begin{bmatrix} \mathbf{S}_{11}^1 & \mathbf{S}_{12}^1 & \mathbf{0} & \mathbf{0} & \mathbf{0} & \cdots & \mathbf{0} \\ \mathbf{S}_{21}^1 & \mathbf{S}_{22}^1+\mathbf{S}_{11}^2 & \mathbf{S}_{12}^2 & \mathbf{0} & \mathbf{0} & \cdots & \mathbf{0} \\ \mathbf{0} & \mathbf{S}_{21}^2 & \mathbf{S}_{22}^2+\mathbf{S}_{11}^3 & \mathbf{S}_{12}^3 & \mathbf{0} & \cdots & \mathbf{0} \\ \mathbf{0} & \mathbf{0} & \mathbf{S}_{21}^3 & \mathbf{S}_{22}^3+\mathbf{S}_{11}^4 & \mathbf{0} & \cdots & \mathbf{0} \\ \mathbf{0} & \mathbf{0} & \mathbf{0} & \mathbf{0} & \ddots & \vdots & \vdots \\ \vdots & \vdots & \vdots & \vdots & \cdots & \mathbf{S}_{22}^{N-1}+\mathbf{S}_{11}^N & \mathbf{S}_{12}^N \\ \mathbf{0} & \mathbf{0} & \mathbf{0} & \mathbf{0} & \cdots & \mathbf{S}_{21}^N & \mathbf{S}_{22}^N \end{bmatrix}. \tag{70}$$

Because $\mathbf{S}_{21}^j = \left(\mathbf{S}_{12}^j\right)^{\mathrm{T}}$, coefficient matrix $\mathcal{A}$ in Eq. (70) is a symmetric matrix. Meanwhile, $\mathcal{A}$ is a sparse matrix, and thus the required computer memory storage can be decreased. Rewriting Eq. (69) as the following form

$$\mathcal{B} = \Psi\rho\mathbf{z} + \Phi, \tag{71}$$

where

$$\Psi = \begin{bmatrix} 0 & \zeta_{12}^1 & 0 & 0 & 0 & \cdots & 0 \\ 0 & \zeta_{22}^1 & \zeta_{12}^2 & 0 & 0 & \cdots & 0 \\ 0 & 0 & \ddots & 0 & 0 & \cdots & 0 \\ 0 & 0 & 0 & \zeta_{22}^{j-1} & \zeta_{12}^j & \cdots & 0 \\ 0 & 0 & 0 & 0 & \ddots & \vdots & \vdots \\ \vdots & \vdots & \vdots & \cdots & 0 & \zeta_{22}^{N-1} & \zeta_{12}^N \\ 0 & 0 & 0 & \cdots & 0 & 0 & \zeta_{22}^N \end{bmatrix}, \tag{72}$$

$$\rho = \begin{bmatrix} -\mathbf{I} & \mathbf{I} & 0 & 0 & 0 & 0 & \cdots & 0 \\ 0 & 0 & -\mathbf{I} & \mathbf{I} & 0 & 0 & \ddots & \vdots \\ \vdots & \ddots & \vdots & \vdots & \vdots & \vdots & 0 & 0 \\ 0 & \cdots & 0 & 0 & 0 & 0 & -\mathbf{I} & \mathbf{I} \end{bmatrix}, \tag{73}$$

$$\mathbf{z} = \left\{\bar{\boldsymbol{\beta}}_0^{\mathrm{T}}, \underline{\boldsymbol{\beta}}_0^{\mathrm{T}}, \bar{\boldsymbol{\beta}}_1^{\mathrm{T}}, \underline{\boldsymbol{\beta}}_1^{\mathrm{T}}, \cdots \bar{\boldsymbol{\beta}}_N^{\mathrm{T}}, \underline{\boldsymbol{\beta}}_N^{\mathrm{T}}\right\}^{\mathrm{T}}, \tag{74}$$

$$\Phi = \left\{\left(\mathbf{x}_0 - \zeta_{11}^1\right)^{\mathrm{T}}, -\left(\zeta_{21}^1 + \zeta_{11}^2\right)^{\mathrm{T}}, \ldots, \right.$$
$$-\left(\zeta_{21}^j + \zeta_{11}^{j+1}\right)^{\mathrm{T}}, \ldots,$$
$$\left. -\left(\zeta_{21}^{N-1} + \zeta_{11}^N\right)^{\mathrm{T}}, -\left(\zeta_{21}^N + \mathbf{x}_{\mathrm{f}}\right)^{\mathrm{T}}\right\}^{\mathrm{T}}. \tag{75}$$

By solving Eq. (67) and taking Eq. (71) into consideration, the costate variable $\boldsymbol{\lambda}$ can be obtained

$$\boldsymbol{\lambda} = \mathcal{A}^{-1}\Psi\rho\mathbf{z} + \mathcal{A}^{-1}\Phi. \tag{76}$$

Then based on Eqs. (38), (49), and (62), we can obtain

$$\mathbf{x}_j = -\mathbf{F}_4^j = -(\mathbf{S}_{21}^j\boldsymbol{\lambda}_{j-1} + \mathbf{S}_{22}^j\boldsymbol{\lambda}_j + \zeta_2^j). \tag{77}$$

Finally, in the current $(k+1)$th iteration step of quasilinearization method, the costate variable $\boldsymbol{\lambda}$ and the state variable $\mathbf{x}$ on all discretization points can be obtained by Eqs. (76) and (77), respectively. When the norm of the state variable $\mathbf{x}$ or the costate variable $\boldsymbol{\lambda}$ in the adjacent iteration step of quasilinearization process satisfies the given precision requirement ε, the quasilinearization process can be stopped. Then substitute the costate variable $\boldsymbol{\lambda}$ of the last iteration step into Eq. (13) and thus the control variable $\mathbf{u}$ can also be obtained.

However, we can see Eq. (76), the costate variable λ is also associated with the unknown variable $\mathbf{z}$ which can only be obtained by solving the linear complementary problem expressed by Eqs. (20)–(23). In the next section, in order to get the numerical solution of costate variable $\boldsymbol{\lambda}$ and construct the closed-loop feedback control scheme, we will add the complementary problem into the above discretization scheme and develop a uniform format that is equivalent to the original nonlinear optimal control problem with finite control input.

3.3 Solution of Hamiltonian boundary-value problem coupled with linear complementary problem

In the $(k+1)$th iteration step, the continuous time domain (t, t_{f}) is divided into N time intervals as shown in Eq. (27). Within a time interval (t_{j-1}, t_j) $(j = 1, 2, \ldots, N)$, the parametric variables $\underline{\boldsymbol{\beta}}$ and $\bar{\boldsymbol{\beta}}$ are approximated as constant vectors $\underline{\boldsymbol{\beta}}_j$ and $\bar{\boldsymbol{\beta}}_j$, and the variables $\bar{\boldsymbol{\alpha}}$ and $\underline{\boldsymbol{\alpha}}$ are approximated as constant vectors $\bar{\boldsymbol{\alpha}}_j$ and $\underline{\boldsymbol{\alpha}}_j$, respectively. We also assume that the linear complementarity condition in Eqs. (20)–(23) is satisfied at discrete time points, i.e.,

$$\bar{\boldsymbol{\alpha}}_j + \mathbf{C}\mathbf{R}^{-1}(t_j)\left(-\mathbf{B}^{\mathrm{T}}(t_j)\boldsymbol{\lambda}_j - \mathbf{C}^{\mathrm{T}}\bar{\boldsymbol{\beta}}_j + \mathbf{C}^{\mathrm{T}}\underline{\boldsymbol{\beta}}_j\right) - \bar{\mathbf{u}} = \mathbf{0}, \tag{78}$$

$$\underline{\boldsymbol{\alpha}}_j - \mathbf{C}\mathbf{R}^{-1}(t_j)\left(-\mathbf{B}^{\mathrm{T}}(t_j)\boldsymbol{\lambda}_j - \mathbf{C}^{\mathrm{T}}\bar{\boldsymbol{\beta}}_j + \mathbf{C}^{\mathrm{T}}\underline{\boldsymbol{\beta}}_j\right) + \mathbf{u} = \mathbf{0}, \tag{79}$$

$$\bar{\boldsymbol{\alpha}}_j \geq \mathbf{0},\ \bar{\boldsymbol{\beta}}_j \geq \mathbf{0}, \bar{\boldsymbol{\alpha}}_j^{\mathrm{T}}\bar{\boldsymbol{\beta}}_j = \mathbf{0}, \tag{80}$$

$$\underline{\boldsymbol{\alpha}}_j \geq \mathbf{0}, \underline{\boldsymbol{\beta}}_j \geq \mathbf{0}, \underline{\boldsymbol{\alpha}}_j^{\mathrm{T}}\underline{\boldsymbol{\beta}}_j = \mathbf{0}. \tag{81}$$

Rewriting Eqs. (78) and (79) as follows

$$\begin{Bmatrix} \bar{\boldsymbol{\alpha}}_j \\ \underline{\boldsymbol{\alpha}}_j \end{Bmatrix} - \mathbf{M}_j \begin{Bmatrix} \bar{\boldsymbol{\beta}}_j \\ \underline{\boldsymbol{\beta}}_j \end{Bmatrix} = \mathrm{E}(t_j)\boldsymbol{\lambda}_j + \begin{Bmatrix} \bar{\mathbf{u}} \\ -\underline{\mathbf{u}} \end{Bmatrix}, \tag{82}$$

where

$$\mathbf{M}_j = \begin{bmatrix} \mathbf{C}\mathbf{R}^{-1}(t_j)\mathbf{C}^{\mathrm{T}} & -\mathbf{C}\mathbf{R}^{-1}(t_j)\mathbf{C}^{\mathrm{T}} \\ -\mathbf{C}\mathbf{R}^{-1}(t_j)\mathbf{C}^{\mathrm{T}} & \mathbf{C}\mathbf{R}^{-1}(t_j)\mathbf{C}^{\mathrm{T}} \end{bmatrix}, \tag{83}$$

$$\mathrm{E}(t_j) = \begin{Bmatrix} \mathbf{C}\mathbf{R}^{-1}(t_j)\mathbf{B}^{\mathrm{T}}(t_j) \\ -\mathbf{C}\mathbf{R}^{-1}(t_j)\mathbf{B}^{\mathrm{T}}(t_j) \end{Bmatrix}. \tag{84}$$

Assembling all the sub-intervals $(j = 1, 2, \ldots, N)$, the following equations can be obtained

$$\boldsymbol{\nu} - \mathbf{M}\mathbf{z} = \mathbf{E}\lambda + \mathbf{U}, \tag{85}$$

$$\boldsymbol{\nu} \geq \mathbf{0}, \quad \mathbf{z} \geq \mathbf{0}, \tag{86}$$

$$\mathbf{z}^{\mathrm{T}}\boldsymbol{\nu} = \mathbf{0}, \tag{87}$$

where

$$\boldsymbol{\nu} = \left\{\bar{\boldsymbol{\alpha}}_0^{\mathrm{T}},\ \underline{\boldsymbol{\alpha}}_0^{\mathrm{T}},\ \bar{\boldsymbol{\alpha}}_1^{\mathrm{T}},\ \underline{\boldsymbol{\alpha}}_1^{\mathrm{T}}, \ldots, \bar{\boldsymbol{\alpha}}_N^{\mathrm{T}},\ \underline{\boldsymbol{\alpha}}_N^{\mathrm{T}}\right\}^{\mathrm{T}}, \tag{88}$$

$$\mathbf{M} = \begin{bmatrix} \mathbf{M}_0 & 0 & \cdots & 0 \\ 0 & \mathbf{M}_1 & \cdots & 0 \\ \vdots & \vdots & \ddots & \vdots \\ 0 & 0 & \cdots & \mathbf{M}_N \end{bmatrix}, \tag{89}$$

$$\mathbf{E} = \begin{bmatrix} \mathbf{E}(t_0) & 0 & \cdots & 0 \\ 0 & \mathbf{E}(t_1) & \cdots & 0 \\ \vdots & \vdots & \ddots & \vdots \\ 0 & 0 & \cdots & \mathbf{E}(t_N) \end{bmatrix}, \tag{90}$$

$$\mathbf{U} = \underbrace{\left\{\bar{\mathbf{u}}^{\mathrm{T}}, -\underline{\mathbf{u}}^{\mathrm{T}},\ \bar{\mathbf{u}}^{\mathrm{T}}, -\underline{\mathbf{u}}^{\mathrm{T}}, \cdots, \bar{\mathbf{u}}^{\mathrm{T}}, -\underline{\mathbf{u}}^{\mathrm{T}}, \cdots, \bar{\mathbf{u}}^{\mathrm{T}}, -\underline{\mathbf{u}}^{\mathrm{T}}\right\}^{\mathrm{T}}}_{2\times N \text{ elements}}. \tag{91}$$

Equations (85)–(87) represent the linear complementary problem, while Eq. (76) represents the solution of the linear HBVP. Thus, we substitute Eq. (76) into Eq. (85) and get the following equation

$$\boldsymbol{\nu} - \mathbf{M}_{\mathrm{new}}\mathbf{z} = \mathbf{q}_{\mathrm{new}}, \tag{92}$$

where

$$\mathbf{M}_{\mathrm{new}} = \mathbf{M} + \mathbf{E}\mathcal{A}^{-1}\Psi\rho, \tag{93}$$

$$\mathbf{q}_{\mathrm{new}} = \mathbf{E}\mathcal{A}^{-1}\Phi + \mathbf{U}. \tag{94}$$

Finally, in the $(k+1)$th iteration step, the linear Hamiltonian boundary-value problem coupled with the linear complementary problem is transformed into the above new form of the linear complementary problem expressed by Eqs. (92), (86), and (87). By solving this new form of the linear complementary problem, the variable $\mathbf{z}$ can be obtained. Then substitute the known variable $\mathbf{z}$ into Eq. (76), the costate variable $\boldsymbol{\lambda}$ can be obtained. Furthermore, substitute $\boldsymbol{\lambda}$ into Eqs. (77) and (13) separately, the state variable $\mathbf{x}$ and the control variable $\mathbf{u}$ can finally be obtained.

To date, the linear HBVP coupled with the linear complementary problem has been solved successfully. From an overall view, the problem that has been solved is the problem in the $(k+1)$ th iteration step after we transformed the original nonlinear optimal control problem with finite control input into the iteration form of linear problems based on the qusilinearization method. After a number of iteration steps, we can finally obtain the state variable $\mathbf{x}$ and control variable $\mathbf{u}$ which can meet the precision requirement.

4 Design and implementation of closed-loop control

In order to realize the goal of closed-loop feedback control, we will design an effective closed-loop feedback control strategy based on the above open-loop optimal control in this section. Assume that the overall feedback step number is Simu_N, then we divide the continuous time domain $\tau \in (t, t_\mathrm{f})$ into Simu_N sub-intervals with equal time step $\vartheta = (t_\mathrm{f} - t)/\mathrm{Simu\_}N$, i.e.,

$$\begin{aligned} t_0^{\mathrm{close}} &= t,\ t_1^{\mathrm{close}} = t+\vartheta,\ \ldots,\ t_i^{\mathrm{close}} \\ &= t + k\vartheta,\ \ldots,\ t_{\mathrm{Simu\_}N}^{\mathrm{close}} = t_\mathrm{f}. \end{aligned} \tag{95}$$

In deed, a closed-loop feedback control strategy is proposed by the fast computing of open-loop optimal problems in different time sub-intervals. In the i th update step of the closed-loop feedback control, we consider the computation of the nonlinear optimal control problem with finite control input in the time sub-intervals $\tau \in \left(t_{i-1}^{\mathrm{close}}, t_\mathrm{f}\right)(1 \le i \le \mathrm{Simu\_}N)$ which can be described as follows

$$\begin{aligned} &\dot{\mathbf{x}}_i^{\mathrm{close}}(\tau) = f\left(\mathbf{x}_i^{\mathrm{close}}(\tau), \mathbf{u}_i^{\mathrm{close}}(\tau)\right), \\ &\mathbf{x}_i^{\mathrm{close}}\left(\tau = t_{i-1}^{\mathrm{close}}\right) = \mathbf{x}_{i-1}^{\mathrm{close}}, \\ &\mathbf{x}_i^{\mathrm{close}}(\tau = t_\mathrm{f}) = \mathbf{x}_\mathrm{f}, \end{aligned} \tag{96}$$

where the control variable $\mathbf{u}_i^{\mathrm{close}}$ is constrained by Eq. (5). The performance index is shown in Eq. (6). Based on the qusilinearization method introduced in Sect. 3.1, the problem described by Eqs. (96), (5), and (6) can be transformed into the iteration form of linear HBVP coupled with linear complementary problem. In the $(k+1)$th iteration of qusilinearization method, the problem can be described as

$$\begin{aligned} &\left(\dot{\mathbf{x}}_i^{\mathrm{close}}\right)^{(k+1)} \\ &= \mathbf{A}^{(k)}(\tau)\left(\mathbf{x}_i^{\mathrm{close}}\right)^{(k+1)} \\ &\quad - \mathbf{B}^{(k)}(\tau)\mathbf{R}^{-1}\left(\mathbf{B}^{(k)}(\tau)\right)^{\mathrm{T}}\left(\boldsymbol{\lambda}_i^{\mathrm{close}}\right)^{(k+1)} \\ &\quad + \mathbf{B}^{(k)}(\tau)\mathbf{u}_\mathrm{d} + \mathbf{w}^{(k)}(\tau) \\ &\quad + \mathbf{B}^{(k)}(\tau)\mathbf{R}^{-1}\mathbf{C}^{\mathrm{T}}\left(\left(\underline{\boldsymbol{\beta}}_i^{\mathrm{close}}\right)^{(k+1)} - \left(\bar{\boldsymbol{\beta}}_i^{\mathrm{close}}\right)^{(k+1)}\right), \end{aligned} \tag{97}$$

$$\begin{aligned} \left(\dot{\boldsymbol{\lambda}}_i^{\mathrm{close}}\right)^{(k+1)} &= -\mathbf{Q}\left(\mathbf{x}_i^{\mathrm{close}}\right)^{(k+1)} \\ &\quad - \left(\mathbf{A}^{(k)}(\tau)\right)^{\mathrm{T}}\left(\boldsymbol{\lambda}_i^{\mathrm{close}}\right)^{(k+1)} + \mathbf{Q}\mathbf{x}_\mathrm{d}, \end{aligned} \tag{98}$$

with the following boundary conditions

$$\left(\mathbf{x}_i^{\mathrm{close}}\right)^{(k+1)}\left(\tau = t_{i-1}^{\mathrm{close}}\right) = \mathbf{x}_{i-1}^{\mathrm{close}}, \tag{99}$$

$$\left(\mathbf{x}_i^{\mathrm{close}}\right)^{(k+1)}(\tau = t_\mathrm{f}) = \mathbf{x}_\mathrm{f}. \tag{100}$$

In order to solve the linear HBVP coupled with linear complementarity problem, based on the discretization scheme introduced in Sect. 3.2, the continuous time domain $\left(t_{i-1}^{\mathrm{close}}, t_\mathrm{f}\right)$ is divided into N sub-intervals with equal time step $\varsigma = \left(t_\mathrm{f} - t_{i-1}^{\mathrm{close}}\right)/N$, i.e.,

$$\begin{aligned} \left(T_i^{\mathrm{close}}\right)_0 &= t_{i-1}^{\mathrm{close}},\ \left(T_i^{\mathrm{close}}\right)_1 \\ &= t_{i-1}^{\mathrm{close}} + \varsigma,\ \ldots,\ \left(T_i^{\mathrm{close}}\right)_j \\ &= t_{i-1}^{\mathrm{close}} + j\varsigma,\ \ldots,\ \left(T_i^{\mathrm{close}}\right)_N = t_\mathrm{f}. \end{aligned} \tag{101}$$

Then, by applying the discretization scheme introduced in Sect. 3.3, the linear HBVP coupled with linear complementary problem can be finally transformed into the following new complementary problem

$$\begin{aligned} &\left(\boldsymbol{\nu}_i^{\mathrm{close}}\right)^{(k+1)} - \left(\left(\mathbf{M}_i^{\mathrm{close}}\right)^{(k+1)}\right)_{\mathrm{new}}\left(\mathbf{z}_i^{\mathrm{close}}\right)^{(k+1)} \\ &= \left(\left(\mathbf{q}_i^{\mathrm{close}}\right)^{(k+1)}\right)_{\mathrm{new}}, \end{aligned} \tag{102}$$

$$\left(\boldsymbol{v}_i^{\text{close}}\right)^{(k+1)} \geq \mathbf{0}, \quad \left(\mathbf{z}_i^{\text{close}}\right)^{(k+1)} \geq \mathbf{0}, \tag{103}$$

$$\left(\left(\mathbf{z}_i^{\text{close}}\right)^{(k+1)}\right)^{\mathrm{T}} \left(\boldsymbol{v}_i^{\text{close}}\right)^{(k+1)} = \mathbf{0}, \tag{104}$$

where

$$\begin{aligned}&\left(\left(\mathbf{M}_i^{\text{close}}\right)^{(k+1)}\right)_{\text{new}}\\ &= \left(\mathbf{M}_i^{\text{close}}\right)^{(k+1)} + \left(\mathbf{E}_i^{\text{close}}\right)^{(k+1)}\\ &\quad \times \left(\left(\mathcal{A}_i^{\text{close}}\right)^{(k+1)}\right)^{-1} \left(\Psi_i^{\text{close}}\right)^{(k+1)} \left(\rho_i^{\text{close}}\right)^{(k+1)},\end{aligned} \tag{105}$$

$$\begin{aligned}&\left(\left(\mathbf{q}_i^{\text{close}}\right)^{(k+1)}\right)_{new}\\ &= \left(\mathbf{E}_i^{\text{close}}\right)^{(k+1)} \left(\left(\mathcal{A}_i^{\text{close}}\right)^{(k+1)}\right)^{-1}\\ &\quad \times \left(\Phi_i^{\text{close}}\right)^{(k+1)} + \left(\mathbf{U}_i^{\text{close}}\right)^{(k+1)}.\end{aligned} \tag{106}$$

By solving the above complementary problem expressed by Eqs. (102)–(104), the variable $\left(\mathbf{z}_i^{\text{close}}\right)^{(k+1)}$ can be obtained. Thus the following open-loop optimal trajectories and costate variables in the $(k+1)$th iteration of qusilinearization method can be get

$$\left(\mathbf{x}_i^{\text{close}}\right)^{(k+1)} = \left\{\left(\mathbf{x}_0^i\right)^{(k+1)}, \left(\mathbf{x}_1^i\right)^{(k+1)}, \ldots, \left(\mathbf{x}_N^i\right)^{(k+1)}\right\}, \tag{107}$$

$$\left(\boldsymbol{\lambda}_i^{\text{close}}\right)^{(k+1)} = \left\{\left(\boldsymbol{\lambda}_0^i\right)^{(k+1)}, \left(\boldsymbol{\lambda}_1^i\right)^{(k+1)}, \ldots, \left(\boldsymbol{\lambda}_N^i\right)^{(k+1)}\right\}. \tag{108}$$

When the norm of the state variable $\mathbf{x}$ or the costate variable $\boldsymbol{\lambda}$ in the adjacent iteration step of quasilinearization process satisfies the given precision requirement ε, the quasilinearization process can be stopped, i.e.,

$$\left\| \left(\mathbf{x}_i^{\text{close}}\right)^{(k+1)} - \left(\mathbf{x}_i^{\text{close}}\right)^{(k)} \right\| \leq \varepsilon, \tag{109}$$

$$\left\| \left(\boldsymbol{\lambda}_i^{\text{close}}\right)^{(k+1)} - \left(\boldsymbol{\lambda}_i^{\text{close}}\right)^{(k)} \right\| \leq \varepsilon, \tag{110}$$

where $||\cdot||$ denotes the norm of a vector. When the iteration ends, the optimal control $\mathbf{u}_i^{\text{close}}$ can be obtained with the known costate variables $\boldsymbol{\lambda}_i^{\text{close}}$ by Eq. (13), and also the following open-loop optimal trajectories and control can be rewritten as

$$\mathbf{x}_i^{\text{close}} = \left\{\mathbf{x}_0^i, \mathbf{x}_1^i, \cdots, \mathbf{x}_N^i\right\}, \tag{111}$$

$$\mathbf{u}_i^{\text{close}} = \left\{\mathbf{u}_0^i, \mathbf{u}_1^i, \cdots, \mathbf{u}_N^i\right\}. \tag{112}$$

Therefore, using only the initial $\mathbf{x}_0^i$ and $\mathbf{u}_0^i$ to integrate the controlled nonlinear differential Eq. (4) in one step, the state variable of the $(i+1)$ th update step of the closed-loop feedback control can be obtained. Thus, the computation of the $(i+1)$ th closed-loop feedback control can be proceeded repeatedly. When all the update steps of the closed-loop feedback control have been computed, the closed-loop trajectory and control expressed by can be obtained. The main part of the closed-loop feedback control strategy can be expressed by the following flowchart (Fig. 3).

5 Numerical simulations

In this section, aiming at the three-dimensional periodic Halo orbits in the Sun–Earth system around the L_2 point, the validity of the proposed numerical algorithm and the optimal feedback control strategy for spacecraft rendezvous are illuminated by numerical simulations. In the first part of this section, the results of open-loop control strategy are given to demonstrate the good properties of the proposed numerical algorithm for solving nonlinear optimal control problem with finite low thrust. The second part of this section shows the results of closed-loop control strategy and test the robustness of the optimal feedback control strategy when dealing with spacecraft rendezvous problems encountering the initial state errors, the perturbations errors of other celestial bodies, and the measurement errors of system states.

All the parameters and detailed data used in the following numerical simulations are summarized in this section: the parameters of CRTBP model for the Sun–Earth/Moon system are given in Table 1; two halo orbits, initial and rendezvous conditions of spacecraft in the same and different family are given in Tables 2 and 3, respectively; simulation parameters of numerical algorithms for solving nonlinear optimal control problem with finite low thrust are given in Table 4.

To measure the rendezvous errors of relative position and velocity with the closed-loop control strategy, the position error Δe_{p} and the velocity error Δe_{v} are defined as

$$\begin{aligned}&\Delta e_{\text{p}x} = \left|x\left(t_{\text{f}}\right) - x^*\left(t_{\text{f}}\right)\right|, \quad \Delta e_{\text{p}y} = \left|y\left(t_{\text{f}}\right) - y^*\left(t_{\text{f}}\right)\right|,\\ &\Delta e_{\text{p}z} = \left|z\left(t_{\text{f}}\right) - z^*\left(t_{\text{f}}\right)\right|,\end{aligned} \tag{113}$$

$$\left\|\Delta e_{\text{p}}\right\| = \sqrt{\Delta e_{\text{p}x}^2 + \Delta e_{\text{p}y}^2 + \Delta e_{\text{p}z}^2}, \tag{114}$$

$$\begin{aligned}&\Delta e_{\text{v}x} = \left|\dot{x}\left(t_{\text{f}}\right) - \dot{x}^*\left(t_{\text{f}}\right)\right|, \quad \Delta e_{\text{v}y} = \left|\dot{y}\left(t_{\text{f}}\right) - \dot{y}^*\left(t_{\text{f}}\right)\right|,\\ &\Delta e_{\text{v}z} = \left|\dot{z}\left(t_{\text{f}}\right) - \dot{z}^*\left(t_{\text{f}}\right)\right|,\end{aligned} \tag{115}$$

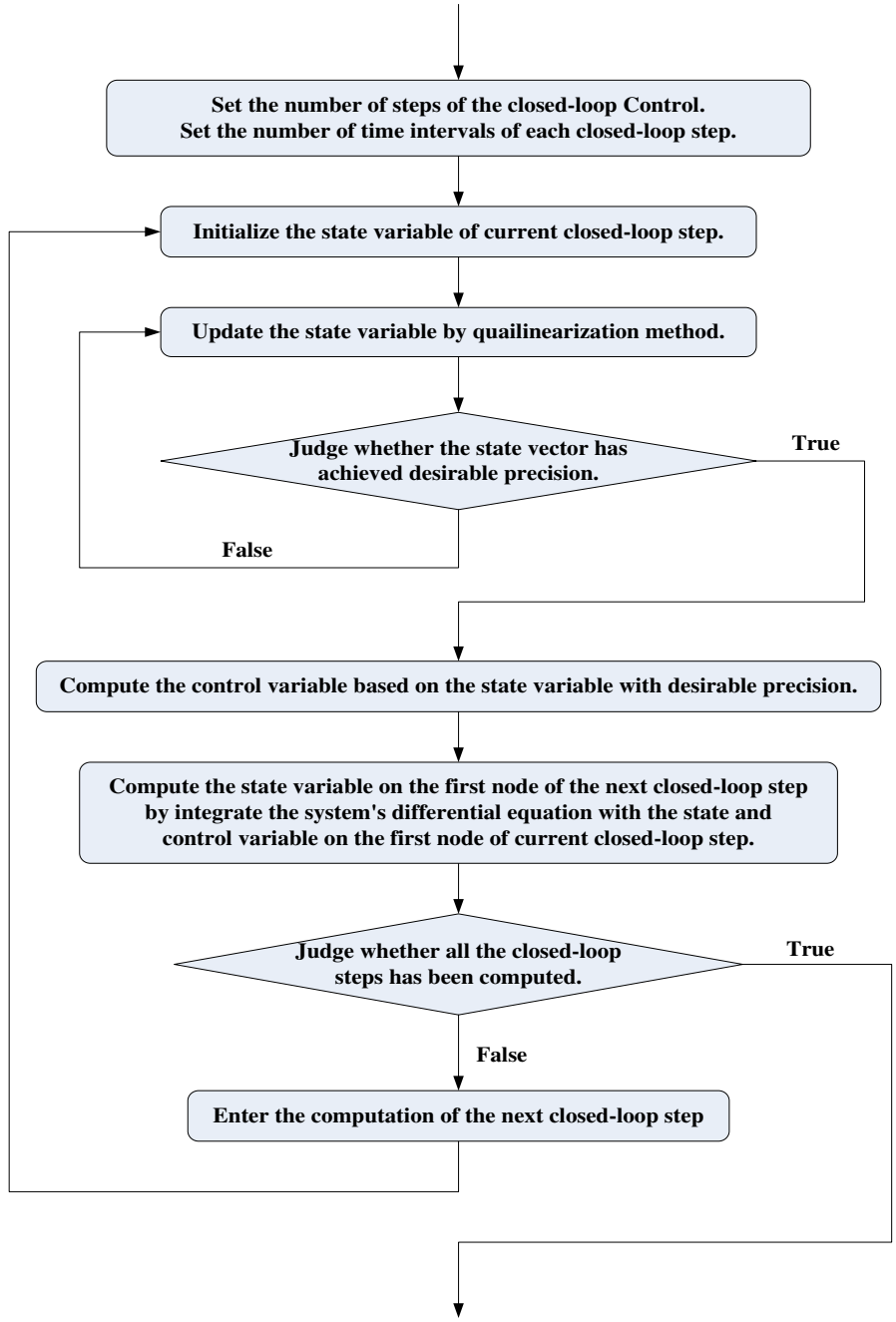

Fig. 3 Flow chart of the proposed closed-loop feedback control scheme

$$\|\Delta e_{\mathrm{v}}\| = \sqrt{\Delta e_{\mathrm{v}x}^2 + \Delta e_{\mathrm{v}y}^2 + \Delta e_{\mathrm{v}z}^2}, \tag{116}$$

where $x\,(t_{\mathrm{f}})$, $y\,(t_{\mathrm{f}})$, and $z\,(t_{\mathrm{f}})$ represent the actual final position, while $x^*\,(t_{\mathrm{f}})$, $y^*\,(t_{\mathrm{f}})$, and $z^*\,(t_{\mathrm{f}})$ are the reference final position in the x, y, and z directions. The final velocity rendezvous error is defined similarly in Eqs. (115) and (116). The final rendezvous position error Δe_{p} is in units of meters, and the final rendezvous velocity error Δe_{v} is in units of meters per second.

5.1 Results of open-loop control

This subsection presents two case studies to demonstrate the open-loop solutions of the nonlinear optimal

Table 1 Parameters of the CRTBP model for the Sun–Earth/Moonsystem

Parameters	Description
μ_E	Earth ratio parameter for the Sun–Earth/Moon system 3.040360×10^{-6}
μ_M	Moon ratio parameter for the Sun–Earth/Moon system 3.694262×10^{-8}
γ	Distance between the Earth and the L_2 libration 1.50767856×10^6 km
L	Distance between the Sun and the Earth barycenter 1.49597871×10^8 km
ω	Mean motion of the Sun–Earth rotating system $1.99098661 \times 10^{-7}$ rad/s
R_M	Mean orbital radius of the Moon 3.942878×10^5 km
ω_M	Mean angular velocity of the Moon 1.547340×10^{-5} rad/s
m_s	Mass of the spacecraft 1,000 kg

Table 2 Initial and rendezvous conditions of spacecraft in the same family

Parameters	Initial halo orbit $\mathbf{x}_0$	Rendezvous halo orbit $\mathbf{x}_d$
x_0 (km)	$-3.8078919497 \times 10^5$	$-5.0396095158 \times 10^5$
y_0 (km)	0	0
z_0	4.1184523753×10^5	5.5231362110×10^5
$\dot{x}_0$	0	0
$\dot{y}_0$ (m/s)	1.2261144053×10^2	1.4649892179×10^2
$\dot{z}_0$	0	0
A_z (km)	5×10^5	7×10^5
T_p (days)	179.5443	178.5487

Table 3 Initial and rendezvous conditions of spacecraft in the different family

Parameters	Initial halo orbit $\mathbf{x}_0$	Rendezvous halo orbit $\mathbf{x}_d$
x_0 (km)	$-2.7817545932 \times 10^5$	$-2.7817545932 \times 10^5$
y_0 (km)	0	0
z_0	2.0051504694×10^5	$-2.0051504694 \times 10^5$
$\dot{x}_0$	0	0
$\dot{y}_0$ (m/s)	1.0144482836×10^2	1.0144482836×10^2
$\dot{z}_0$	0	0
A_z (km)	2.5×10^5	-2.5×10^5
T_p (days)	180.1966	180.1966

control problem with finite low thrust for the spacecraft rendezvous problem. The case A_1 means the spacecraft rendezvous in the same family of halo orbits. The case A_2 means the spacecraft rendezvous in the different family of Halo orbits. The detailed data for initial and rendezvous conditions of spacecraft are given in Tables 3 and 4, respectively. In the process of quasi linearization for the proposed numerical algorithm, the guesses for initial iteration control inputs are simply chosen to be zero over the entire time domain, whereas all the guesses for initial iteration states are arbitrarily set to the initial values of $\mathbf{x}_0$. All computations were performed in MATLAB (R2010a) (on an Intel® Core™ 2 Quad Q9400 machine with a 2.66 GHz processor and 3 GB of RAM). In each of the above two cases, the open-loop control of spacecraft rendezvous problem is discretized with 100 nodes and the optimal solution is obtained within 5 s.

Table 4 Simulation parameters of numerical algorithm for spacecraft rendezvous

Parameters	Value
Upper limit of control input: $\underline{\mathbf{u}}$	$\left[0.12N\ 0.12N\ 0.12N\right]^{\mathrm{T}}$
Lower limit of control input: $\bar{\mathbf{u}}$	$-\left[0.12N\ 0.12N\ 0.12N\right]^{\mathrm{T}}$
Terminal constraint control: $\mathbf{u}_d$	$\left[0\ 0\ 0\right]^{\mathrm{T}}$
Coefficient matrix: $\mathbf{C}$	$\mathbf{I}_3$
Weight matrix: $\mathbf{Q}$	$\mathbf{I}_6$
Weight matrix: $\mathbf{R}$	$\mathbf{I}_3$

Figures 4 and 5 show the results of spacecraft rendezvous trajectory and control thrust under the open-loop optimal control for the cases A_1 and A_2. In Figs. 4a and 5a, pursuit spacecraft from the initial point can successfully rendezvous objective spacecraft moving steadily on objective halo orbit. Additionally, the directions of thrust show that the rendezvous trajectories are moving along the direction of Halo orbits. In Figs. 4b and 5b, the time histories of optimal control profiles, i.e., finite low thrusts are presented with respect to the rendezvous time (95 and 87 days, respectively). The maximum amplitude of low thrust appears on the initial and terminal of rendezvous time, and they all satisfy the constraint of control inputs. Tables 5 and 6 give the absolute errors of adjacent iteration steps of the proposed numerical algorithm for solving the nonlinear optimal control problem with finite low thrust. With a few iteration steps, the proposed numerical algorithm can converge to very high accuracy. Therefore,

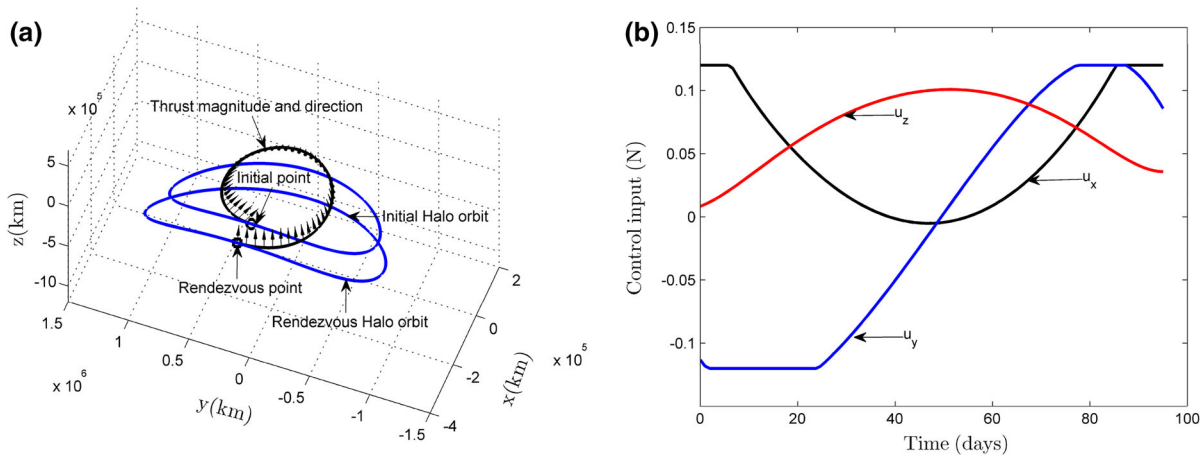

Fig. 4 Results of open-loop control for the case A_1:**a** trajectory, **b** thrust

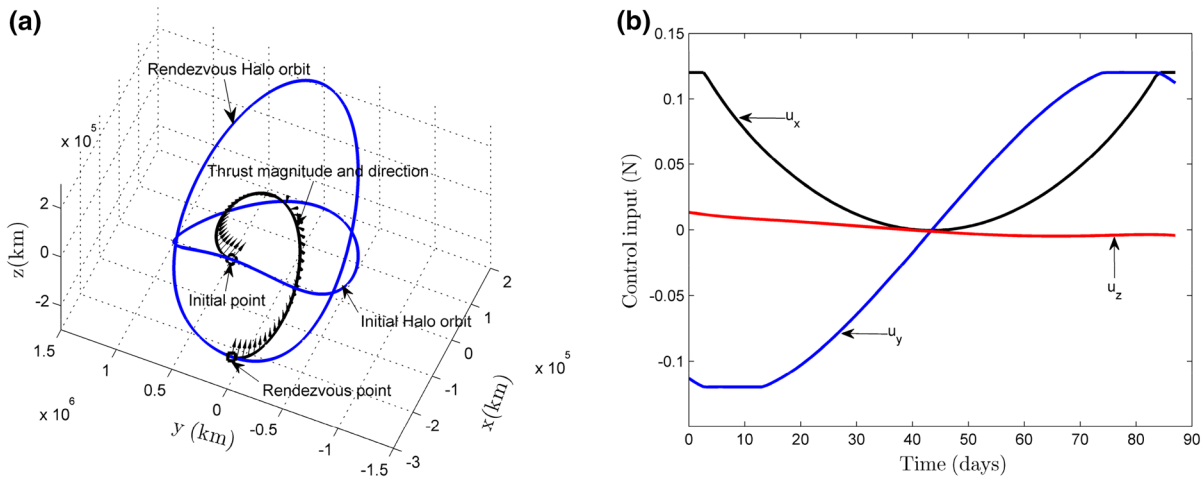

Fig. 5 Results of open-loop control for the case A_2: **a** trajectory, **b** thrust

Table 5 Absolute errors of adjacent iteration steps for the case A_1

k	$\left\|J^k - J^{k-1}\right\|$	$\left\|\mathbf{x}^k - \mathbf{x}^{k-1}\right\|$	$\left\|\boldsymbol{\lambda}^k - \boldsymbol{\lambda}^{k-1}\right\|$	$\left\|\mathbf{u}^k - \mathbf{u}^{k-1}\right\|$
1	5.7616	15.0630	36.4904	12.5827
3	9.2600×10^{-2}	1.6110×10^{-1}	3.0650×10^{-1}	9.5050×10^{-1}
5	1.7622×10^{-4}	1.5000×10^{-3}	4.0000×10^{-3}	5.3000×10^{-3}
7	1.8827×10^{-6}	1.5770×10^{-5}	4.0844×10^{-5}	5.2807×10^{-5}
9	1.9068×10^{-8}	1.7357×10^{-7}	4.5034×10^{-7}	5.6133×10^{-7}
11	1.9607×10^{-10}	2.1921×10^{-9}	5.6781×10^{-9}	7.1489×10^{-9}
13	7.9066×10^{-12}	3.4465×10^{-11}	1.6910×10^{-10}	1.1519×10^{-10}

the proposed numerical algorithm has a character of high accuracy.

To gain an insight into the dynamics character of spacecraft rendezvous between the halo orbits, Fig. 6 shows the time histories of state variables under the open-loop optimal control for ideal and actual environments. The time histories of state variables from the actual environments including perturbations of the

Table 6 Absolute errors of adjacent iteration steps for the case A_2

k	$\left\|J^k - J^{k-1}\right\|$	$\left\|\mathbf{x}^k - \mathbf{x}^{k-1}\right\|$	$\left\|\boldsymbol{\lambda}^k - \boldsymbol{\lambda}^{k-1}\right\|$	$\left\|\mathbf{u}^k - \mathbf{u}^{k-1}\right\|$
1	3.7069	12.1001	16.8131	13.8600
3	2.7680×10^{-1}	3.4440×10^{-1}	5.2250×10^{-1}	2.8687
5	1.5790×10^{-5}	2.2684×10^{-4}	2.4505×10^{-4}	1.2000×10^{-3}
7	1.0250×10^{-8}	1.4860×10^{-7}	1.5249×10^{-7}	7.6814×10^{-7}
9	6.7120×10^{-12}	1.0218×10^{-10}	4.4458×10^{-9}	5.2781×10^{-10}
11	1.5321×10^{-13}	7.3826×10^{-12}	8.3468×10^{-11}	1.5780×10^{-11}

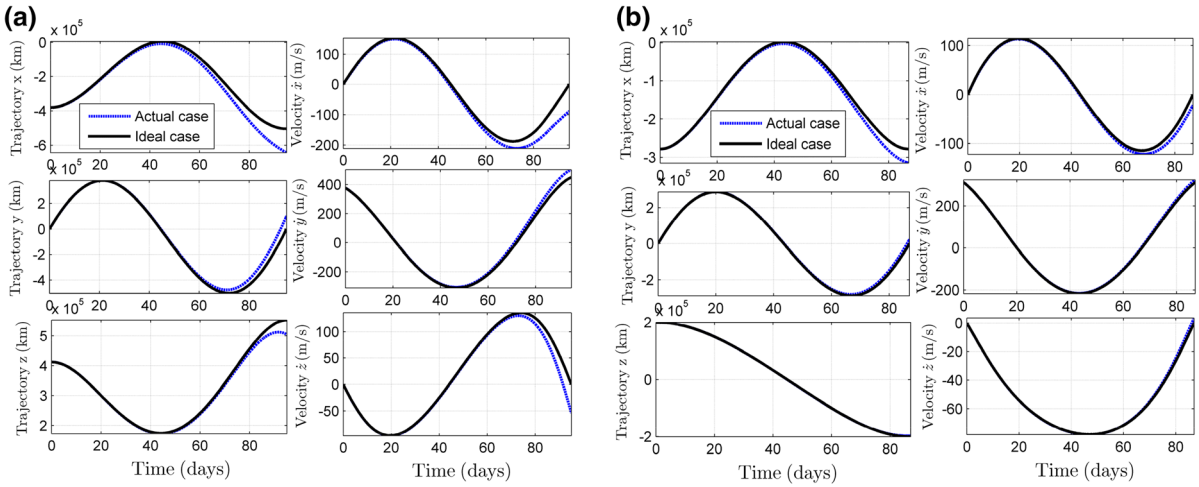

Fig. 6 Comparisons of open-loop control between ideal and actual cases: **a** case A_1 and **b** case A_2

Moon in CRTBP have obvious differences from the ideal environments without perturbations of the Moon. The pursuit spacecraft can not rendezvous the objective spacecraft in such actual environments. Therefore, from a practical point of view, the closed-loop feedback control of spacecraft rendezvous between the Halo orbits is important and should be further investigated.

5.2 Results of closed-loop control

In addition to perturbations of the Moon in CRTBP of the Sun–Earth system, disturbance in real environments of spacecraft's mission is inevitably introduced due to parameter uncertainties, sensor measurement errors, or combination of different errors and can considerably degrade the performance of the spacecraft's mission. This subsection presents four kinds of disturbance error studies to demonstrate the robustness and performance of the closed-loop feedback control strategy of spacecraft rendezvous problem with finite low thrust between the halo orbits.

The first kind of disturbance error is the initial state error, i.e., case B_i: assuming that the objective spacecraft is moving steadily on the objective halo orbit, and the pursuit spacecraft has an initial position error of 1 km and an initial velocity error of 1 m/s.

The second kind of disturbance error is perturbations error, i.e., case C_i: because the effects of the Moon in CRTBP of the Sun–Earth system are also ignored, the bicircular four-body model is more realistic than the Sun–Earth CRTBP models. It describes the dynamics observed in systems such as the environment near the Earth and describes the motion of a spacecraft of negligible mass under the gravitational force of the Sun, Earth, and Moon. The Sun and Earth revolve in circular orbits around their center of mass (barycenter), and the Moon moves in a circular orbit around the center of the Earth. Therefore, perturbations of the Moon are taken into the simulation of the closed-loop feedback control strategy of spacecraft rendezvous problem. The detailed description and formulae for the bicircular four-body model can be found in Ref. [12].

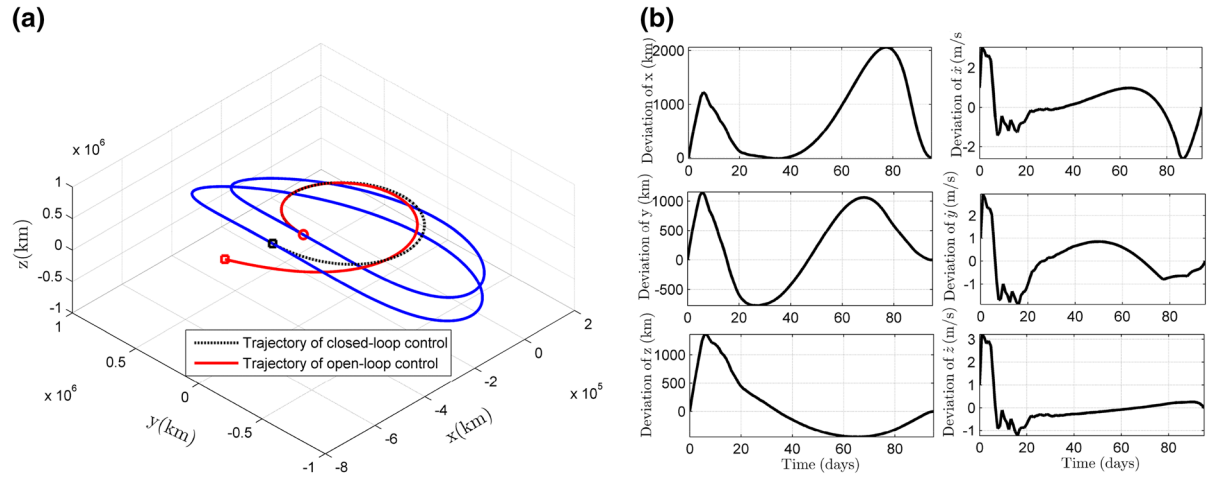

Fig. 7 Case E_1: comparisons of open-loop and closed-loop control: **a** trajectory and **b** derivations

The third kind of disturbance error is measurement error, i.e., case D_{i}: measurement errors or navigation errors, comes from the navigational equipment and measurement methods, which is assumed to be in regard with the distance between the pursuit spacecraft and the objective spacecraft. These navigation errors or measurement errors are incorporated into the simulation of the closed-loop feedback control strategy of spacecraft rendezvous problem. We made simulation studies with 3 km initial position measurement noise and 3 m/s initial velocity measurement noise. Both noises experience exponential decay in regard with the relative distance between two spacecrafts.

The fourth kind of disturbance error is combination of all the above errors, i.e., case E_{i}: in order to test the robustness and validity of the closed-loop feedback control strategy in extreme situation, the initial state errors, the perturbations errors, and the measurement errors are all incorporated into the simulation of the closed-loop feedback control strategy for this case.

In the above cases $i = 1, 2$, when $i = 1$, it means the spacecraft rendezvous in the same family of Halo orbits, and when $i = 2$, it means the spacecraft rendezvous in the different family of Halo orbits. In all cases of numerical simulations for the closed-loop feedback control of spacecraft rendezvous problem, the detailed data for initial and rendezvous conditions of spacecraft are employed as the same with the open-loop optimal control. Meanwhile, in the process of quasilinearization for the proposed numerical algorithm, the guesses for initial iteration control inputs and initial iteration states are also the same as the open-loop optimal control. In each of the above cases, the closed-loop feedback control of spacecraft rendezvous problem is discretized and implemented with 100 steps. During the numerical propagations of spacecraft's states, simulations are conducted by linearly interpolating a discrete optimal control solution and using the MATLAB ODE45 function to propagate the state between the time steps. The absolute and relative error tolerances of ODE45 function are set to be 1×10^{-12}.

Figures 7 and 8 give the comparisons of open-loop and closed-loop control for the case E_1 and E_2, respectively. As shown in Figs. 7a and 8a, the pursuit spacecraft controlled by the open-loop optimal control strategy cannot meet the objective spacecraft at the final time under the disturbances. However, the proposed closed-loop feedback control strategy is capable of counteracting the disturbances and achieving the desired rendezvous results. In the presence of disturbance, the trajectory from the closed-loop feedback control changes repeatedly and a new optimal trajectory is feedback to the system as each feedback instant. The derivations between the trajectory of closed-loop feedback control with disturbances and the trajectory of open-loop optimal control without disturbances are shown in Figs. 7b and 8b. There are obvious derivations in the middle of the rendezvous trajectory. But the derivations are nearly zero at the final derivations time due to the closed-loop feedback control. It means that the disturbances have important effect on spacecraft rendezvous and cannot be ignored.

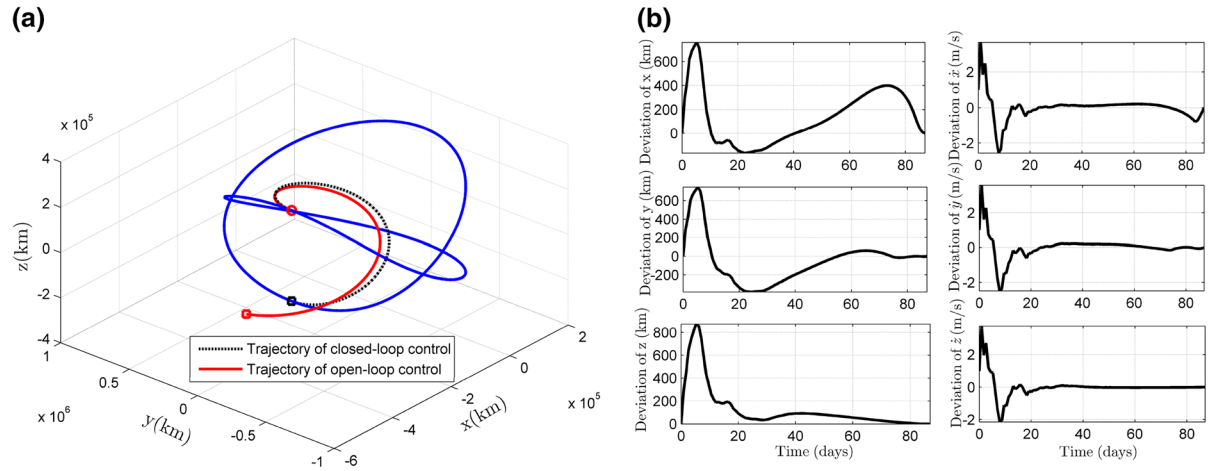

Fig. 8 Case E_2: comparisons of open-loop and closed-loop control:**a** trajectory and **b** derivations

Table 7 Robustness test of different cases in the same family of Halo orbits

Cases	Δe_{px}	Δe_{py}	Δe_{pz}	$\|\Delta e_p\|$	$\Delta \bar{e}_{vx}$	$\Delta \bar{e}_{vy}$	$\Delta \bar{e}_{vz}$	$\|\Delta \bar{e}_v\|$
Initial state error: B_1	1.860	0.764	0.710	2.012	1.291	0.070	0.014	1.293
Perturbations errors: C_1	3.010	0.767	0.072	3.107	3.950	0.119	0.006	3.951
Measurement errors: D_1	2.419	0.467	0.368	2.491	2.062	0.268	0.344	2.108
All the above errors: E_1	3.338	0.342	0.479	3.389	4.374	0.350	0.477	4.413

where $\Delta \bar{e}_{vx} = \Delta e_{vx} \times 10^5$, $\Delta \bar{e}_{vy} = \Delta e_{vy} \times 10^5$, $\Delta \bar{e}_{vz} = \Delta e_{vz} \times 10^5$, $\Delta \bar{e}_v = \Delta e_v \times 10^5$

Table 8 Robustness test of different cases in the different family of Halo orbits

cases	Δe_{px}	Δe_{py}	Δe_{pz}	$\|\Delta e_p\|$	$\Delta \bar{e}_{vx}$	$\Delta \bar{e}_{vy}$	$\Delta \bar{e}_{vz}$	$\|\Delta \bar{e}_v\|$
Initial state error: B_2	0.795	0.329	0.018	0.860	1.108	0.066	0.006	1.110
Perturbations errors: C_2	1.532	0.334	0.020	1.567	3.100	0.093	0.008	3.101
Measurement errors: D_2	1.177	1.183	1.503	2.603	1.528	1.901	1.994	3.150
All the above errors: E_2	0.695	1.045	0.702	1.437	1.789	0.949	0.898	2.215

where $\Delta \bar{e}_{vx} = \Delta e_{vx} \times 10^5$, $\Delta \bar{e}_{vy} = \Delta e_{vy} \times 10^5$, $\Delta \bar{e}_{vz} = \Delta e_{vz} \times 10^5$, $\Delta \bar{e}_v = \Delta e_v \times 10^5$

Tables 7 and 8 show the detailed data for the robustness test of different cases in the same and different family of Halo orbits, respectively. From the two Tables we can see that the pursuit spacecraft controlled by the closed-loop feedback control strategy can meet the objective spacecraft at the final time under the different kinds of disturbance error. Furthermore, the maximum rendezvous position error is less than 4 m, and the maximum rendezvous velocity error is less than 5×10^{-5} m/s. Therefore, we can conclude that the proposed closed-loop feedback control strategy with the initial state errors, the perturbations errors of the Moon, and the measurement errors of system states have stronger robustness and high rendezvous accuracy.

The robustness and high accuracy of the proposed closed-loop feedback control strategy have been shown in the above discussions. From a practical point of view, there are some issues that deserve further investigation. For example, success of this closed-loop feedback control strategy depends heavily on relatively fast computation speed. It is a common practice for real-time optimal control to maximize computational efficiency by using as few as possible discretization intervals.

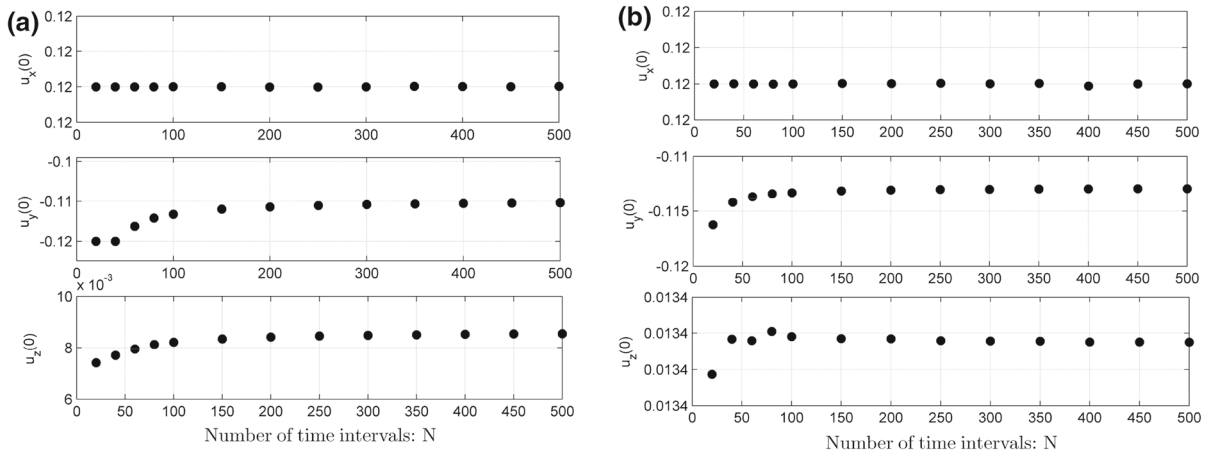

Fig. 9 Comparisons of open-loop control on initial control using different number of time intervals: **a** case A_1 and **b** case A_2

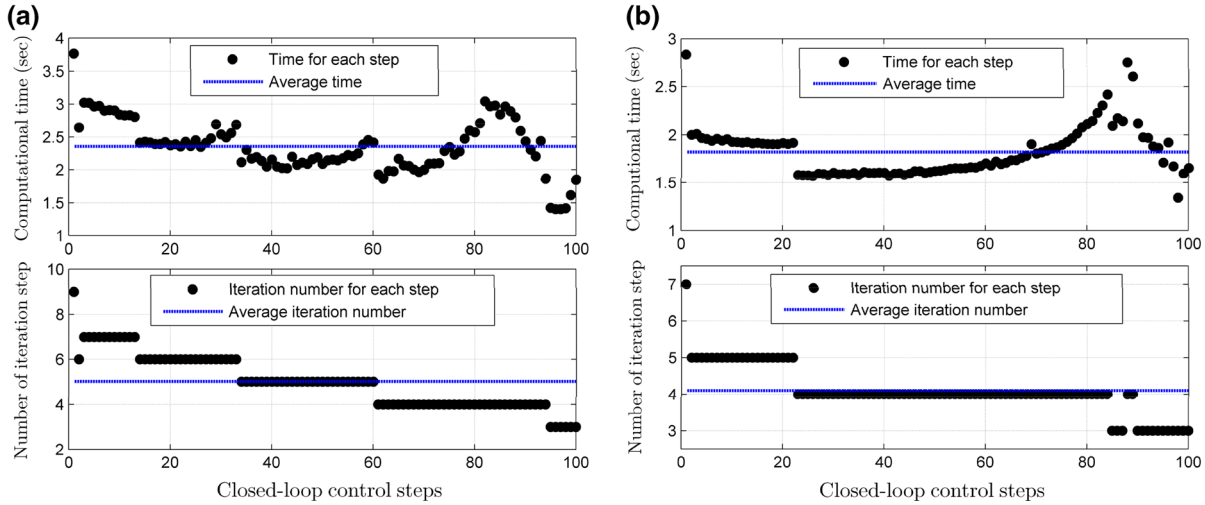

Fig. 10 Comparisons of closed-loop control on online computational time and number of iteration step: **a** case E_1 and **b** case E_2

However, a minimum number of discretization intervals must be enforced to meet the precision requirement of a practical mission. Because the closed-loop feedback control strategy is implemented by online open-loop optimal control at each feedback instant, the initial inputs should receive special attention.

In Fig. 9, the cases A_1 and A_2 are selected to compute and compare $u_x(0)$, $u_y(0)$, and $u_z(0)$ which are solved by using different numbers of discretization intervals. For both cases A_1 and A_2, the solutions of initial control are tending toward stability as long as the number of discretization intervals is greater than 100. Therefore, the solution obtained from the open-loop optimal control with 100 discretization intervals is taken as a reference for further comparison, which reveals that the computational time and number of iterations are of high efficiency in the closed-loop feedback control strategy at each feedback instant.

Figure 10 gives the comparisons of closed-loop feedback control on online computational time and number of iteration step with 100 discretization intervals. Computation of the first open-loop optimal control takes 2.5–4 s and 7–9 iterations, and the subsequent open-loop optimal control updates are computed within approximately 1.5–3 s and 3–7 iterations depending on the disturbance induced by the initial state errors, the perturbations errors of the Moon, the measurement

errors of system states, and the stability of the Windows environment at the time of run.

At last, it should be noted that application of the closed-loop feedback control introduced in this paper does not require the prior knowledge of the reference rendezvous trajectory for feedback control. Therefore, the computation time and memory for the reference rendezvous trajectory can be saved. More importantly, when the spacecrafts have obvious derivation from the reference rendezvous trajectory, the success of the rendezvous mission can also be guaranteed by the proposed closed-loop feedback control strategy.

6 Conclusions

In this paper, the nonlinear closed-loop feedback control idea has been introduced to solve the problem of spacecraft rendezvous between libration orbits in the presence of the gravitational forces from the Moon, the navigational error, and the actuator saturation limits as well. Successive open-loop optimal control solutions for the spacecraft rendezvous are used to construct a sampled-data closed-loop feedback control law. A new numerical algorithm is proposed for rapidly solving open-loop optimal control problem by the resulting sparse symmetrical linear equation coupled with linear complementary problem. Theoretical analysis shows that one important feature of the proposed control scheme is that it requires no prior knowledge of the reference rendezvous trajectory for feedback control. Meanwhile, it provides the capability of recovering from failure with rapid trajectory reshaping. Simulations indicate that rapid re-computation of the open-loop optimal control can effectively be used for online optimal control of spacecrafts rendezvous in the presence of various disturbances and uncertainties. The robustness and high precision of the proposed controller are also demonstrated through several case studies. As shown in the simulation results, the proposed closed-loop feedback control strategy not only guarantees high precision for spacecraft rendezvous under the four kinds of disturbances, but also enjoys dominant real-time merits, which are critical for practical applications.

Moreover, the proposed numerical algorithms for open-loop optimal control and the closed-loop feedback control strategy are quite general. They apply not only to the spacecraft rendezvous between the Halo orbits, but also intercepting, repairing, rescuing, and docking as well. For instance, they can be employed to implement the Lissajous orbits and figure-eight orbits intercepting in the Sun–Earth/Moon system.

Acknowledgments The authors are grateful for the financial support of the National Science Foundation of China (11102031), Fundamental Research Funds for Central Universities (DUT13LK25), Program Funded by Liaoning Province Education Administration (L2013015), and the National Basic Research Program of China (2010CB832704).

Appendix: The detailed expression of the formulae in some equations

It is easy to verify that the elements $\mathbf{K}_{u,v}^{j}$ $(u, v = 1, 2, 3, 4)$ and $\mathbf{f}_{i}^{j}$ $(i = 1, 2, 3, 4)$ in Eqs. (35)–(38) can be given by

$$\mathbf{K}_{11}^{j} = \int_{t_{j-1}}^{t_j} N_1 N_1 \left[\mathbf{B}(\tau)\mathbf{R}^{-1}(\tau)\mathbf{B}^{\mathrm{T}}(\tau)\right]\mathrm{d}\tau, \tag{117}$$

$$\mathbf{K}_{12}^{j} = \int_{t_{j-1}}^{t_j} N_1 \left[(\dot{\mathbf{M}}\otimes\mathbf{I}) - (\mathbf{M}\otimes\mathbf{A}(\tau))\right]\mathrm{d}\tau = \left(\mathbf{K}_{21}^{j}\right)^{\mathrm{T}}, \tag{118}$$

$$\mathbf{K}_{13}^{j} = \int_{t_{j-1}}^{t_j} N_1 \left[\underline{\mathbf{N}}\otimes\mathbf{B}(\tau)\mathbf{R}^{-1}(\tau)\mathbf{B}^{\mathrm{T}}(\tau)\right]\mathrm{d}\tau = \left(\mathbf{K}_{31}^{j}\right)^{\mathrm{T}}, \tag{119}$$

$$\mathbf{K}_{14}^{j} = \int_{t_{j-1}}^{t_j} N_1 N_n \left[\mathbf{B}(\tau)\mathbf{R}^{-1}(\tau)\mathbf{B}^{\mathrm{T}}(\tau)\right]\mathrm{d}\tau = \left(\mathbf{K}_{41}^{j}\right)^{\mathrm{T}}, \tag{120}$$

$$\begin{aligned}\mathbf{f}_{1}^{j} = &-\int_{t_{j-1}}^{t_j} \mathbf{N}_1\mathbf{B}(\tau)\mathbf{u}_{\mathrm{d}}\mathrm{d}\tau - \int_{t_{j-1}}^{t_j} \mathbf{N}_1\mathbf{w}(\tau)\mathrm{d}\tau \\ &-\left(\int_{t_{j-1}}^{t_j} \mathbf{N}_1\mathbf{B}(\tau)\mathbf{R}^{-1}\mathbf{C}^{T}\mathrm{d}\tau\right)\left(\underline{\beta}^{j}\text{-}\bar{\beta}^{j}\right),\end{aligned} \tag{121}$$

$$\mathbf{K}_{22}^{j} = \int_{t_{j-1}}^{t_j} \left[\mathbf{M}^{\mathrm{T}}\mathbf{M}\otimes\mathbf{Q}(\tau)\right]\mathrm{d}\tau, \tag{122}$$

$$\mathbf{K}_{23}^{j} = \int_{t_{j-1}}^{t_j} \left[\left(\underline{\mathbf{N}}\dot{\mathbf{M}}^{\mathrm{T}}\otimes\mathbf{I}\right) - \left(\underline{\mathbf{N}}\mathbf{M}^{\mathrm{T}}\otimes\mathbf{A}^{\mathrm{T}}(\tau)\right)\right]\mathrm{d}\tau = \left(\mathbf{K}_{32}^{j}\right)^{\mathrm{T}}, \tag{123}$$

$$\mathbf{K}_{24}^{j} = \int_{t_{j-1}}^{t_j} N_n \left[\left(\dot{\mathbf{M}}^{\mathrm{T}}\otimes\mathbf{I}\right) - \left(\mathbf{M}^{\mathrm{T}}\otimes\mathbf{A}^{\mathrm{T}}(\tau)\right)\right]\mathrm{d}\tau = \left(\mathbf{K}_{42}^{j}\right)^{\mathrm{T}}, \tag{124}$$

$$\mathbf{f}_2^j = \int_{t_{j-1}}^{t_j} (\mathbf{M} \otimes \mathbf{I})^{\mathrm{T}} \mathbf{Q}(\tau) \mathbf{x}_{\mathrm{d}} \mathrm{d}\tau, \tag{125}$$

$$\mathbf{K}_{33}^j = \int_{t_{j-1}}^{t_j} \left[\underline{\mathbf{N}}^{\mathrm{T}} \underline{\mathbf{N}} \otimes \mathbf{B}(\tau) \mathbf{R}^{-1}(\tau) \mathbf{B}^{\mathrm{T}}(\tau) \right] \mathrm{d}\tau, \tag{126}$$

$$\mathbf{K}_{34}^j = \int_{t_{j-1}}^{t_j} N_n \left[\left(\underline{\mathbf{N}}^{\mathrm{T}} \otimes \mathbf{B}(\tau) \mathbf{R}^{-1}(\tau) \mathbf{B}^{\mathrm{T}}(\tau) \right) \right] \mathrm{d}\tau = \left(\mathbf{K}_{43}^j \right)^{\mathrm{T}}, \tag{127}$$

$$\mathbf{f}_3^j = -\int_{t_{j-1}}^{t_j} \underline{\mathbf{N}}^{\mathrm{T}} \otimes \mathbf{B}(\tau) \mathbf{u}_{\mathrm{d}} \mathrm{d}\tau - \int_{t_{j-1}}^{t_j} \underline{\mathbf{N}}^{\mathrm{T}} \otimes \mathbf{w}(\tau) \mathrm{d}\tau - \left(\int_{t_{j-1}}^{t_j} \underline{\mathbf{N}}^{\mathrm{T}} \otimes \mathbf{B}(\tau) \mathbf{R}^{-1} \mathbf{C}^T \mathrm{d}\tau \right) \left(\underline{\boldsymbol{\beta}}^j - \bar{\boldsymbol{\beta}}^j \right), \tag{128}$$

$$\mathbf{K}_{44}^j = \int_{t_{j-1}}^{t_j} N_n N_n \left[\mathbf{B}(\tau) \mathbf{R}^{-1}(\tau) \mathbf{B}^{\mathrm{T}}(\tau) \right] \mathrm{d}\tau, \tag{129}$$

$$\mathbf{f}_4^j = -\int_{t_{j-1}}^{t_j} \mathbf{N}_n \mathbf{B}(\tau) \mathbf{u}_{\mathrm{d}} \mathrm{d}\tau - \int_{t_{j-1}}^{t_j} \mathbf{N}_n \mathbf{w}(\tau) \mathrm{d}\tau - \left(\int_{t_{j-1}}^{t_j} \mathbf{N}_n \mathbf{B}(\tau) \mathbf{R}^{-1} \mathbf{C}^T \mathrm{d}\tau \right) \left(\underline{\boldsymbol{\beta}}^j - \bar{\boldsymbol{\beta}}^j \right). \tag{130}$$

Similarly, it is easy to verify that the elements ζ_{pq}^j $(p, q = 1, 2)$ in Eqs. (58)–(59) can be given by

$$\begin{aligned}
\zeta_{11}^j = & -\left(\mathbf{E}_u^{\mathrm{T}} + \mathbf{K}_{12}^j \right) \left(\mathbf{K}_{22}^j \right)^{-1} \\
& \times \left(\mathbf{K}_{23}^j \left(\mathbf{K}_{aa}^j \right)^{-1} \mathbf{K}_{32}^j \left(\mathbf{K}_{22}^j \right)^{-1} \mathbf{f}_2^j - \mathbf{f}_2^j \right) \\
& + \left(\mathbf{E}_u^{\mathrm{T}} + \mathbf{K}_{12}^j \right) \left(\mathbf{K}_{22}^j \right)^{-1} \mathbf{K}_{23}^j \left(\mathbf{K}_{aa}^j \right)^{-1} \\
& \times \left(\int_{t_{j-1}}^{t_j} \underline{\mathbf{N}}^{\mathrm{T}} \otimes \mathbf{B}(\tau) \mathbf{u}_{\mathrm{d}} \mathrm{d}\tau + \int_{t_{j-1}}^{t_j} \underline{\mathbf{N}}^{\mathrm{T}} \otimes \mathbf{w}(\tau) \mathrm{d}\tau \right) \\
& - \mathbf{K}_{13}^j \left(\mathbf{K}_{aa}^j \right)^{-1} \mathbf{K}_{32}^j \left(\mathbf{K}_{22}^j \right)^{-1} \mathbf{f}_2^j + \mathbf{K}_{13}^j \left(\mathbf{K}_{aa}^j \right)^{-1} \\
& \times \left(\int_{t_{j-1}}^{t_j} \underline{\mathbf{N}}^{\mathrm{T}} \otimes \mathbf{B}(\tau) \mathbf{u}_{\mathrm{d}} \mathrm{d}\tau + \int_{t_{j-1}}^{t_j} \underline{\mathbf{N}}^{\mathrm{T}} \otimes \mathbf{w}(\tau) \mathrm{d}\tau \right) \\
& - \int_{t_{j-1}}^{t_j} \mathbf{N}_1 \mathbf{B}(\tau) \mathbf{u}_{\mathrm{d}} \mathrm{d}\tau - \int_{t_{j-1}}^{t_j} \mathbf{N}_1 \mathbf{w}(\tau) \mathrm{d}\tau,
\end{aligned} \tag{131}$$

$$\begin{aligned}
\zeta_{12}^j = & -\left(\mathbf{E}_u^{\mathrm{T}} + \mathbf{K}_{12}^j \right) \left(\mathbf{K}_{22}^j \right)^{-1} \mathbf{K}_{23}^j \left(\mathbf{K}_{aa}^j \right)^{-1} \\
& \times \int_{t_{j-1}}^{t_j} \underline{\mathbf{N}}^{\mathrm{T}} \otimes \mathbf{B}(\tau) \mathbf{R}^{-1} \mathbf{C}^{\mathrm{T}} \mathrm{d}\tau \\
& - \mathbf{K}_{43}^j \left(\mathbf{K}_{aa}^j \right)^{-1} \int_{t_{j-1}}^{t_j} \underline{\mathbf{N}}^{\mathrm{T}} \otimes \mathbf{B}(\tau) \mathbf{R}^{-1} \mathbf{C}^{\mathrm{T}} \mathrm{d}\tau \\
& + \int_{t_{j-1}}^{t_j} \mathbf{N}_1 \mathbf{B}(\tau) \mathbf{R}^{-1} \mathbf{C}^{\mathrm{T}} \mathrm{d}\tau,
\end{aligned} \tag{132}$$

$$\begin{aligned}
\zeta_{21}^j = & -\left(\mathbf{K}_{42}^j - \mathbf{E}_{\mathrm{d}}^{\mathrm{T}} \right) \left(\mathbf{K}_{22}^j \right)^{-1} \\
& \times \left(\mathbf{K}_{23}^j \left(\mathbf{K}_{aa}^j \right)^{-1} \mathbf{K}_{32}^j \left(\mathbf{K}_{22}^j \right)^{-1} \mathbf{f}_2^j - \mathbf{f}_2^j \right) \\
& + \left(\mathbf{K}_{42}^j - \mathbf{E}_{\mathrm{d}}^{\mathrm{T}} \right) \left(\mathbf{K}_{22}^j \right)^{-1} \mathbf{K}_{23}^j \left(\mathbf{K}_{aa}^j \right)^{-1} \\
& \times \left(\int_{t_{j-1}}^{t_j} \underline{\mathbf{N}}^{\mathrm{T}} \otimes \mathbf{B}(\tau) \mathbf{u}_{\mathrm{d}} \mathrm{d}\tau + \int_{t_{j-1}}^{t_j} \underline{\mathbf{N}}^{\mathrm{T}} \otimes \mathbf{w}(\tau) \mathrm{d}\tau \right) \\
& - \mathbf{K}_{43}^j \left(\mathbf{K}_{aa}^j \right)^{-1} \mathbf{K}_{32}^j \left(\mathbf{K}_{22}^j \right)^{-1} \mathbf{f}_2^j + \mathbf{K}_{43}^j \left(\mathbf{K}_{aa}^j \right)^{-1} \\
& \times \left(\int_{t_{j-1}}^{t_j} \underline{\mathbf{N}}^{\mathrm{T}} \otimes \mathbf{B}(\tau) \mathbf{u}_{\mathrm{d}} \mathrm{d}\tau + \int_{t_{j-1}}^{t_j} \underline{\mathbf{N}}^{\mathrm{T}} \otimes \mathbf{w}(\tau) \mathrm{d}\tau \right) \\
& - \int_{t_{j-1}}^{t_j} \mathbf{N}_n \mathbf{B}(\tau) \mathbf{u}_{\mathrm{d}} \mathrm{d}\tau - \int_{t_{j-1}}^{t_j} \mathbf{N}_n \mathbf{w}(\tau) \mathrm{d}\tau
\end{aligned} \tag{133}$$

$$\begin{aligned}
\zeta_{22}^j = & -\left(\mathbf{K}_{42}^j - \mathbf{E}_{\mathrm{d}}^{\mathrm{T}} \right) \left(\mathbf{K}_{22}^j \right)^{-1} \mathbf{K}_{23}^j \left(\mathbf{K}_{aa}^j \right)^{-1} \\
& \times \int_{t_{j-1}}^{t_j} \underline{\mathbf{N}}^{\mathrm{T}} \otimes \mathbf{B}(\tau) \mathbf{R}^{-1} \mathbf{C}^{\mathrm{T}} \mathrm{d}\tau \\
& - \mathbf{K}_{43}^j \left(\mathbf{K}_{aa}^j \right)^{-1} \int_{t_{j-1}}^{t_j} \underline{\mathbf{N}}^{\mathrm{T}} \otimes \mathbf{B}(\tau) \mathbf{R}^{-1} \mathbf{C}^{\mathrm{T}} \mathrm{d}\tau \\
& + \int_{t_{j-1}}^{t_j} \mathbf{N}_n \mathbf{B}(\tau) \mathbf{R}^{-1} \mathbf{C}^{\mathrm{T}} \mathrm{d}\tau.
\end{aligned} \tag{134}$$

References

1. Gómez, G., Lo, M.W., Masdemont, J.J.: Libration Point Orbits and Applications, World Scientific Publishing (2003)
2. Aram, A., Zohoor, H., Sohrabpour, S.: Space station on spatial periodic orbits around the Moon. Sci. Iran. B. **18**(3), 393–397 (2011)

3. Raftery, M., Hoffman, J.: International space station as a base camp for exploration beyond low Earth orbit. Acta. Astronaut. **85**(4–5), 25–32 (2013)
4. Li, Z., Yang, X.B., Gao, H.J.: Autonomous impulsive rendezvous for spacecraft under orbital uncertainty and thruster faults. J. Frankl. Inst. Eng. Appl. Math. **350**(9), 2455–2473 (2012)
5. Gao, X.Y., Teo, K.L., Duan, G.R.: Robust H∞ control of spacecraft rendezvous on elliptical orbit. J. Frankl. Inst. Eng. Appl. Math. **349**(8), 2515–2529 (2012)
6. Luo, Y.Z., Zhang, J., Li, H.Y., Tang, G.J.: Interactive optimization approach for optimal impulsive rendezvous using primer vector and evolutionary algorithms. Acta. Astronaut. **67**(3–4), 396–405 (2010)
7. Luo, Y.Z., Liang, L.B., Wang, H., Tang, G.J.: Quantitative performance for spacecraft rendezvous trajectory safety. J. Guid. Control Dyn. **34**(4), 1264–1269 (2011)
8. Volle, M.: Optimal variable-specific-impulse rendezvous trajectories between Halo orbits. In: 19th International Symposium on Space Flight Dynamics. Japan Society for Aeronautical and Space Sciences and ISTS, Kanazawa, Japan (2006)
9. Marinescu, A., Nicolae, A., Dumitrache, M.: Optimal low-thrust libration points rendezvous in Earth-moon system. In: AIAA Guidance, Navigation, and Control Conference and Exhibit, AIAA-99-4050, Portland, USA, pp. 535–540 (1999)
10. Marinescu, A., Dumitrache, M.: The nonlinear problem of the optimal libration points rendezvous in Earth-moon system. In: AIAA/AAS Astrodynamics Specialist Conference, AIAA-2000-4433, Denver, USA, pp. 564–571 (2000)
11. Peng, H.J., Yang, C.F., Li, Y.P., Zhang, S., Chen, B.S.: Surrogate-based parameter optimization and optimal control for optimal trajectory of Halo orbit rendezvous. Aerosp. Sci. Technol. **26**(1), 176–184 (2013)
12. Salmani, M., Büskens, C.: Real-time control of optimal low-thrust transfer to the Sun–Earth L1 halo orbit in the bicircular four-body problem. Acta. Astronaut. **69**(9–10), 882–891 (2011)
13. Xin, M., Balakrishnan, S.N., Pernicka, H.J.: Multiple spacecraft formation control with θ-D method. IET Control Theory Appl. **1**(2), 485–493 (2007)
14. Hu, Q.L.: Robust adaptive sliding mode attitude maneuvering and vibration damping of three-axis-stabilized flexible spacecraft with actuator saturation limits. Nonlinear Dyn. **55**(4), 301–321 (2009)
15. Yang, X.B., Cao, X.B., Gao, H.J.: Sampled-data control for relative position holding of spacecraft rendezvous with thrust nonlinearity. IEEE Trans. Ind. Electron. **59**(2), 1146–1153 (2012)
16. Lian, Y.J., Meng, Y.H., Tang, G.J., Liu, L.H.: Constant-thrust glideslope guidance algorithm for time-fixed rendezvous in real halo orbit. Acta. Astronaut. **79**, 241–252 (2012)
17. Wen, H., Jin, D.P., Hu, H.Y.: Optimal feedback control of the deployment of a tethered subsatellite subject to perturbations. Nonlinear Dyn. **51**(4), 501–514 (2008)
18. Wen, H., Jin, D.P., Hu, H.Y.: Infinite-horizon control for retrieving a tethered subsatellite via an elastic tether. J. Guid. Control Dyn. **31**(4), 899–906 (2008)
19. Awrejcewicz, J., Tomczak, K., Lamarque, C.-H.: Controlling system with impacts. Int. J. Bifurc. Chaos **9**(3), 547–553 (1999)
20. Betts, J.T.: Survey of numerical methods for trajectory optimization. J. Guid. Control Dyn. **21**(2), 193–207 (1998)
21. Conway, B.A.: A survey of methods available for the numerical optimization of continuous dynamic systems. J. Optim. Theory. Appl. **152**(2), 271–306 (2012)
22. Williams, P.: Application of pseudospectral methods for receding horizon control. J. Guid. Control Dyn. **27**(2), 310–314 (2004)
23. Yan, H., Fahroo, F., Ross, I.M.: Optimal feedback control laws by Legendre pseudospectral approximations. In: Proceedings of the American Control Conference, Arlington, USA, pp. 2388–2393 (2001)
24. Guo, T., Jiang, F.H., Li, J.F.: Homotopic approach and pseudospectral method applied jointly to low thrust trajectory optimization. Acta. Astronaut. **71**(2–3), 38–50 (2012)
25. Andrianov, I.V., Awrejcewicz, J.: Solutions in the Fourier series form, Gibbs phenomena and Padé approximants. J. Sound. Vib. **245**(4), 753–756 (2001)
26. Peng, H.J., Gao, Q., Wu, Z.G., Zhong, W.X.: Efficient sparse approach for solving receding-horizon control problems. J. Guid. Control Dyn. **36**(6), 1864–1872 (2013)
27. Arnold, V.I.: Mathematical Methods of Classical Mechanics. Springer, New York (1989)
28. Peng, H.J., Gao, Q., Wu, Z.G., Zhong, W.X.: Symplectic approaches for solving two-point boundary-value problems. J. Guid. Control Dyn. **35**(2), 653–658 (2012)